APPENDIX M

Modeling Protocol & Attainment Demonstration for the 2022 Eastern Kern Ozone State Implementation Plan

Modeling Protocol & Attainment Demonstration for the 2022 Eastern Kern Ozone State Implementation Plan

Prepared by
California Air Resources Board
Eastern Kern Air Pollution Control District

Prepared for
United States Environmental Protection Agency Region IX

September 2022

Table of Contents

I. Introduction .....**Error! Bookmark not defined.**

II. Methodology.....**Error! Bookmark not defined.**

A. Meteorological Modeling ..... **Error! Bookmark not defined.**

B. Emissions..... **Error! Bookmark not defined.**

C. Air Quality Modeling..... **Error! Bookmark not defined.**

III. Results.....**Error! Bookmark not defined.**

A. Meteorological Model Evaluation ..... **Error! Bookmark not defined.**

B. Phenomenological Evaluation ..... **Error! Bookmark not defined.**

C. Air Quality Model Evaluation..... **Error! Bookmark not defined.**

D. Air Quality Model Diagnostic Evaluation ..... **Error! Bookmark not defined.**

E. Future Design Values in 2026 and 2032 ..... **Error! Bookmark not defined.**

F. NOx/VOC Sensitivity Analysis for Reasonable Further Progress (RFP)**Error! Bookmark not defined.**

G. Unmonitored Area Analysis..... **Error! Bookmark not defined.**

References .....**Error! Bookmark not defined.**

IV. Supplemental Materials.....**Error! Bookmark not defined.**

List of Figures

Figure 1. Map of California (left) along with the location of Eastern Kern County Nonattainment Area (EKNA) in magenta. The shaded and gray line contours denote the gradients in topography (km). The outer box of the top panel is the California statewide 12 km modeling domain, while the inner box shows the 4 km modeling domain covering Central California. The insert on the bottom shows a zoomed-in view of the spatial extent (magenta lines) and approximate regional boundary of the EKNA and the location of ozone and meteorological monitoring sites (circle markers) in its vicinity. ..... **Error! Bookmark not defined.**

Figure 2. Trends in summer emissions of NOx and ROG (tons per day) between 2000 and 2020 in Eastern Kern, Western Kern and Los Angeles Counties. Anthropogenic emissions estimates are from the California Emission Projection Model (CEPAM) 2019 Ozone SIP Baseline Projection Version 1.04 with 2017 base year. 2018 biogenic ROG emissions are from MEGAN 3.0 biogenic model calculations. Note that emissions are represented on a log scale, which can mask small changes in the emissions. ..... **Error! Bookmark not defined.**

Figure 3. Trends in Eastern Kern's Maximum Daily Average 8-hour Ozone Design Value (ppb) and 70 ppb 8-hour Ozone NAAQS exceedance days between 2000 and 2020.....**Error! Bookmark not defined.**

Figure 4. Example showing how the location of the MDA8 ozone for the top ten days in the reference and future years are chosen. ..... **Error! Bookmark not defined.**

Figure 5. WRF modeling domains (D01 36 km; D02 12 km; and D03 4 km)... **Error! Bookmark not defined.**

Figure 6. Monthly average biogenic ROG emissions for 2018 in the EKNA. .. **Error! Bookmark not defined.**

Figure 7. Monthly average soil NOx emissions for 2018 in the EKNA ..... **Error! Bookmark not defined.**

Figure 8. Meteorological monitoring sites utilized in the model evaluation for Eastern Kern. Numbers reflect the sites listed in Table 7. ..... **Error! Bookmark not defined.**

Figure 9. Distribution of daily mean bias (left) and mean error (right) from April –October 2018. Results are shown for wind speed (top), temperature (middle), and RH (bottom).....**Error! Bookmark not defined.**

Figure 10. Spatial distribution of mean bias (left) and mean error (right) for April-October 2018. Results are shown for wind speed (top), temperature (middle), and RH (bottom).....**Error! Bookmark not defined.**

Figure 11. Comparison of modeled and observed hourly wind speed (left), 2-meter temperature (center), and relative humidity (right), April – October 2018. ..... **Error! Bookmark not defined.**

Figure 12. Surface wind field at 13:00 PST (top) and 20:00 PST (bottom) on August 07, 2018. Modeled wind field is shown with black wind vectors, while observations are shown in red. ..... **Error! Bookmark not defined.**

Figure 13. Average wind field at 5:00 PST (top) and 13:00 PST (bottom) for the top 10 observed ozone days at Mojave monitor in 2018. Modeled wind field is shown with black wind vectors, while observations are shown in red. ..... **Error! Bookmark not defined.**

Figure 14. Observed (left) and modeled (right) wind roses at the Mojave site for the top 10 observed ozone days in 2018. ..... **Error! Bookmark not defined.**

Figure 15. Modeled and observed at 12:00 UTC (top) and 00:00 UTC (bottom) 500 hPa geopotential height for the top 10 observed ozone days in 2018. . **Error! Bookmark not defined.**

Figure 16. Comparison of various statistical metrics from the model attainment demonstration modeling to the range of statistics from the 69 peer-reviewed studies summarized in Simon et al (2012). (MDA denotes Maximum Daily Average). Red circular markers show statistics calculated from modeled ozone at the monitor location, while blue triangular markers show statistics calculate from the maximum ozone in the 3x3 array of grid cells surrounding the monitor. ..... **Error! Bookmark not defined.**

Figure 17. Average MDA8 ozone for the top 10 ozone days in 2018 from the model simulations overlaid with observation data (SJV and SoCAB sites marked as circle, Mojave-923PooleSt marked as triangle), where the top 10 days from the observations were chosen based on the Mojave-923PooleSt site. ..... **Error! Bookmark not defined.**

Figure 18. Illustration of a typical ozone isopleth plot, where each line represents ozone mixing ratio, in 10 ppb increments, as a function of initial NOx and VOC (or ROG) mixing ratio (adapted from Seinfeld and Pandis, 1998, Figure 5.15). General chemical regimes for ozone formation are shown as NOx-disbenefit (red circle), transitional (blue circle), and NOx-limited (green circle). ..... **Error! Bookmark not defined.**

Figure 19. Site-specific average weekday and weekend maximum daily average 8-hour ozone for each year from 2000 to 2020 in the EKNA. The colored circle markers denote observed values while the black square, triangle add diamond markers denote the simulated baseline 2018, future years 2026 and 2032 values. Points falling below the 1:1 dashed line represent a NO_x-disbenefit regime, those on the 1:1 dashed line represent a transitional regime, and those above the 1:1 dashed line represent a NO_x-limited regime. ..... **Error! Bookmark not defined.**

Figure 20. Spatial distribution of the future 2026 DVs (left) and 2032 DVs (right) based on the unmonitored area analysis in the EKNA. ..... **Error! Bookmark not defined.**

Figure 21. Spatial distribution of the future 2026 DVs (left) and 2032 DVs (right) based on the unmonitored area analysis in the EKNA, with fire days excluded in DVs calculation for EKNA and SJV sites. 49

Figure 22. Terrain plots of EKNA and surrounding regions, with mark of grids that have interpolated 2026 Ozone concentration above standard (75 ppb) based on the unmonitored area analysis in the EKNA. Blue bordered grids in the figures represent the area that have interpolated

2026 ozone concentration above standard (75 ppb), with fire days included (left) and excluded (right) in DVs calculation for EKNA and SJV sites. 50

List of Tables

Table 1. Data from each year that are utilized in the Design Value calculation for a specific year (DV Year), and the yearly weighting of data for the average Design Value calculation (or DV_R). ..... **Error! Bookmark not defined.**

Table 2. Year-specific 8-hour ozone design values for 2018, 2019 and 2020, and the average baseline design value (DV_R, represented as the average of three design values) for 2018 at the Mojave site located in the EKNA. The 2020 DV is the two-year average of the 4th highest 8-hour O_3 concentrations from 2018 and 2019. ..... **Error! Bookmark not defined.**

Table 3. WRF vertical layer structure..... **Error! Bookmark not defined.**

Table 4. WRF Physics options. ..... **Error! Bookmark not defined.**

Table 5. EKNA Summer Planning Emissions for 2018, 2026, and 2032 (tons/day). .....**Error! Bookmark not defined.**

Table 6. CMAQ configuration and settings. ..... **Error! Bookmark not defined.**

Table 7. Meteorological site location and parameter measured. ... **Error! Bookmark not defined.**

Table 8. Hourly surface wind speed, temperature and relative humidity statistics for April through October, 2018. IOA denotes index of agreement. ..... **Error! Bookmark not defined.**

Table 9. Maximum daily average 8-hour ozone performance statistics in the EKNA for the 2018 ozone season (April - October). Maximum daily average 8-hour ozone with simulated data extracted at grid cell where the monitor is located. ..... **Error! Bookmark not defined.**

Table 10. Maximum daily average 8-hour ozone performance statistics in the EKNA for the 2018 ozone season (April - October). Maximum daily average 8-hour ozone with simulated data extracted from the 3x3 grid cell array maximum centered at the monitor. .. **Error! Bookmark not defined.**

Table 11. Maximum daily average 1-hour ozone performance statistics in the EKNA for the 2018 ozone season (April - October). Maximum daily average 1-hour ozone with simulated data extracted at grid cell where the monitor is located. ..... **Error! Bookmark not defined.**

Table 12. Maximum daily average 1-hour ozone performance statistics in the EKNA for the 2018 ozone season (April - October). Maximum daily average 1-hour ozone with simulated data extracted from the 3x3 grid cell array maximum centered at the monitor. .. **Error! Bookmark not defined.**

Table 13. Hourly ozone performance statistics in the EKNA for the 2018 ozone season (April - October). Hourly ozone with simulated data extracted at grid cell where the monitor is located. Note that only statistics for the grid cell in which the monitor is located were calculated for hourly ozone. ..... **Error! Bookmark not defined.**

Table 14. Summary of key parameters related to the future year 2026 ozone design value (DV) calculation. ..... **Error! Bookmark not defined.**

Table 15. Summary of key parameters related to the future year 2032 ozone design value (DV) calculation. ..... **Error! Bookmark not defined.**

Table 16. Summary of the ozone improvement from the 45% emissions reductions at the monitoring site in the EKNA. ..... **Error! Bookmark not defined.**

Acronyms

ADAM – Aerometric Data Analysis and Management
AQMIS – Air Quality and Meteorological Information System
ARB – Air Resources Board
BCs – Boundary Conditions
CAM-Chem – Community Atmosphere Model with Chemistry
CEPAM – California Emissions Projection Analysis Model
CESM – Community Earth System Model
CMAQ Model – Community Multi-scale Air Quality Model
CTM – Chemical Transport Model
DV – Design Value
EKNA – Eastern Kern county Non-attainment Area
HD I/M – Heavy-Duty Vehicle Inspection and Maintenance
ICs – Initial Conditions
IOA – Index of Agreement
LA – Los Angeles
LAI – Leaf Area Index
MB – Mean Bias
MCIP – Meteorology-Chemistry Interface Processor
MDAB – Mojave Desert Air Basin
MDA8 – Maximum Daily Average 8-hour Ozone
ME – Mean Error
MEGAN – Model of Emissions of Gases and Aerosols
MFB – Mean Fractional Bias
MFE – Mean Fractional Error
MOZART – Model for Ozone and Related chemical Tracers
NAAQS – National Ambient Air Quality Standard
NASA – National Aeronautics and Space Administration
NARR - North American Regional Reanalysis
NCAR – National Center for Atmospheric Research
NMB – Normalized Mean Bias

NME – Normalized Mean Error

NAAQS – National Ambient Air Quality Standards

NOAA - National Oceanic and Atmospheric Administration

NO_x – Oxides of nitrogen

OGV – Ocean Going Vessels

R – Correlation coefficient

R^2 – R-squared/Coefficient of determination

RH – Relative Humidity

RMSE – Root Mean Square Error

ROG – Reactive Organic Gases

RRF – Relative Response Factor

SAPRC – Statewide Air Pollution Research Center

SIP – State Implementation Plan

SJV – San Joaquin Valley

SJVAB – San Joaquin Valley Air Basin

SoCAB – South Coast Air Basin

U.S. EPA – United States Environmental Protection Agency

VOCs – Volatile Organic Compounds

WRF Model – Weather and Research Forecast Model

I. Introduction

The Eastern Kern County Non-attainment Area (EKNA) encompasses an area of 3,707 square miles and is home to ~132,000 residents (Figure 1). It is geographically situated in the eastern half of Kern County on the western edge of the Mojave Desert Air Basin (MDAB) and extends from the Sierra-Nevada mountains and Transverse Ranges in the northwest and southwest, respectively, to the Searles Valley and Valley Wells to the north, and the Mojave Desert and Antelope Valley in the east and south, respectively. The mountain ranges to the northwest and southwest separate the sparsely populated EKNA from the more densely populated areas in the Southern San Joaquin Valley Air Basin (SJVAB) and Northern South Coast Air Basin (SoCAB). However, mountain passes such as the Tehachapi and Soledad Canyon/Cajon passes that connect MDAB to SJV and SoCAB, respectively, facilitate the transport of emissions and pollutants into the region.

Due to its location in the northwest of the Mojave Desert, the climate of Eastern Kern is similar to that of a desert, but not as extreme, and quite different from regions located in the coastal areas such as Los Angeles. The elevation of the area varies between ~700-1000 meters above sea level and has low humidity. Summer months are generally hot and dry, and the winter months are cool and wet. The average high temperatures generally stay in the 90s (°F) and 60s (°F) in the summer and winter months, respectively. The average annual rainfall is less than 6 inches with most of the rainfall occurring in the winter months. Both winter and summer seasons can experience periods of high pressure and stagnation, which are conducive to pollutant buildup. The local sources of pollution along with polluted air masses from the nearby regions (SJVAB and SoCAB) that are frequently transported into this area through mountain passes tend to stagnate over Eastern Kern under unfavorable meteorological conditions, resulting in high ozone levels, which exceed the U.S. EPA 2008 and 2015 National Ambient Air Quality Standards (NAAQS) for 8-hour ozone. Furthermore, in regions like the EKNA the absence of large sources of fresh Oxides of nitrogen (NO_x) emissions at night prevents the removal of ozone through the NO_x titration process, and allows the nighttime ozone levels to remain elevated. This can facilitate pollutant carryover the following morning, and can also contribute to elevated ozone levels on the following day.

Summer emission trends from 2000 to 2020 in the EKNA are shown in Figure 2 for anthropogenic NOx and Reactive Organic Gases (ROG), along with summer biogenic ROG emissions in the EKNA averaged from May to October 2018 (green circle marker). Figure 2 clearly shows a significant decrease in both local anthropogenic NOx (from 39.6 tpd to 19.2 tpd) and ROG (from 11.8 tpd to 7.4 tpd) emissions from 2000 to 2020. While the ROG emissions declined steadily throughout the entire 20 year period, the decline in NOx emissions slowed significantly after 2009. In 2018, biogenic ROG (49.5 tpd) is estimated to be ~6 times higher than the corresponding anthropogenic emissions (7.7 tpd) in the EKNA.

The transport of pollutants from the SJVAB and SoCAB can significantly contribute to the exceedances of the federal ozone NAAQS in the EKNA. As such, it is useful to examine the

emissions trend in Western Kern County (i.e., SJV portion of Kern County) and Los Angeles (LA) County of SoCAB as well. The anthropognic NOx and ROG emissions trends for Western Kern and LA County are also displayed in Figure 2 and show a substantial decline in emissions from 2000 to 2020. However, these upwind source regions exhibit much higher emissions compared to local sources in EKNA. For 2018, the Western Kern anthropogenic NOx and ROG emissions are estimated to be 49.5 tpd and 64.7 tpd, which are ~2.5 and 8 times higher than the corresponding local emissions in EKNA. The biogenic ROG emissions in Western Kern are estimated to be ~110 tpd for 2018, which is more than twice of the corresponding biogenic emissions (49.5 tpd) in the EKNA. Similarly, the LA County anthropogenic NOx and ROG emissions for the year 2018 are estimated to be 221.6 and 252.8 tpd, which are ~11.5 and ~33 times higher than the corresponding emissions in the EKNA. The biogenic ROG emissions in LA County are estimated to be 128 tpd and ~2.5 times higher than the corresponding anthropogenic emissions (49.5 tpd) in the EKNA. It can be clearly seen from Figure 2 that the upwind source regions have emissions that are an order of magnitude or higher than the local emissions, and when aided by conducive meteorological conditions that facilitate pollutant transport, can be the dominant contributor to ozone levels in this region (EKAPCD, 2003).

Over the same 2000 to 2020 time period, the 8-hour ozone design value (DV) within the EKNA declined steadily (Figure 3), but also exhibited a fair amount of variability due to year-to-year differences in meteorology, which impacts the transport of pollutants from upwind sources and the associated changes in biogenic emissions. Overall, the area-wide design values have declined by ~11 ppb from 97 ppb in 2000 to 86 ppb in 2020, albeit with fluctuations due to the year-to-year meteorological variability. However, these DVs are still substantially higher than the current 2015 70 ppb and the 2008 75 ppb 8-hour ozone standards. Exceedances of the 70 ppb standard in the EKNA (Figure 3 bottom panel) have substantially declined over time from 81 in 2000 to 18 in 2020 indicating significant improvements in ozone air quality across the region. In recent years, the prevalence of forest fires during the summer ozone season significantly impacted the air quality in the EKNA. High ozone concentrations were observed at EKNA's Mojave PooleSt monitor and other surrounding sites in the upwind SJVAB and SCAB on days impacted by forest fires (see Weight of Evidence section of the SIP document) and likely caused the increase in the DVs seen from 2018 to 2020. To remove the impact of forest fires in 2018 and 2020, ozone DVs were calculated by excluding high ozone days that were impacted by forest fires. Details of the fire impact days can be found in the Weight of Evidence analysis. Excluding the fire impacts, ozone DVs would be 81 ppb, 78 ppb and 77 ppb in 2018, 2019 and 2020, respectively, and are denoted by black circle markers in the top panel of Figure 3. The number of exceedance days also dropped to 44 (from 53) and 14 (from 18) in 2018 and 2020 when the forest fire impacted days were excluded (black triangle markers in bottom panel of Figure 3).

Figure 1. Map of California (left) along with the location of Eastern Kern County Nonattainment Area (EKNA) in magenta. The shaded and gray line contours denote the gradients in topography (km). The outer box of the top panel is the California statewide 12 km modeling domain, while the inner box shows the 4 km modeling domain covering Central California. The insert on the bottom shows a zoomed-in view of the spatial extent (magenta lines) and approximate regional boundary of the EKNA and the location of ozone and meteorological monitoring sites (circle markers) in its vicinity.

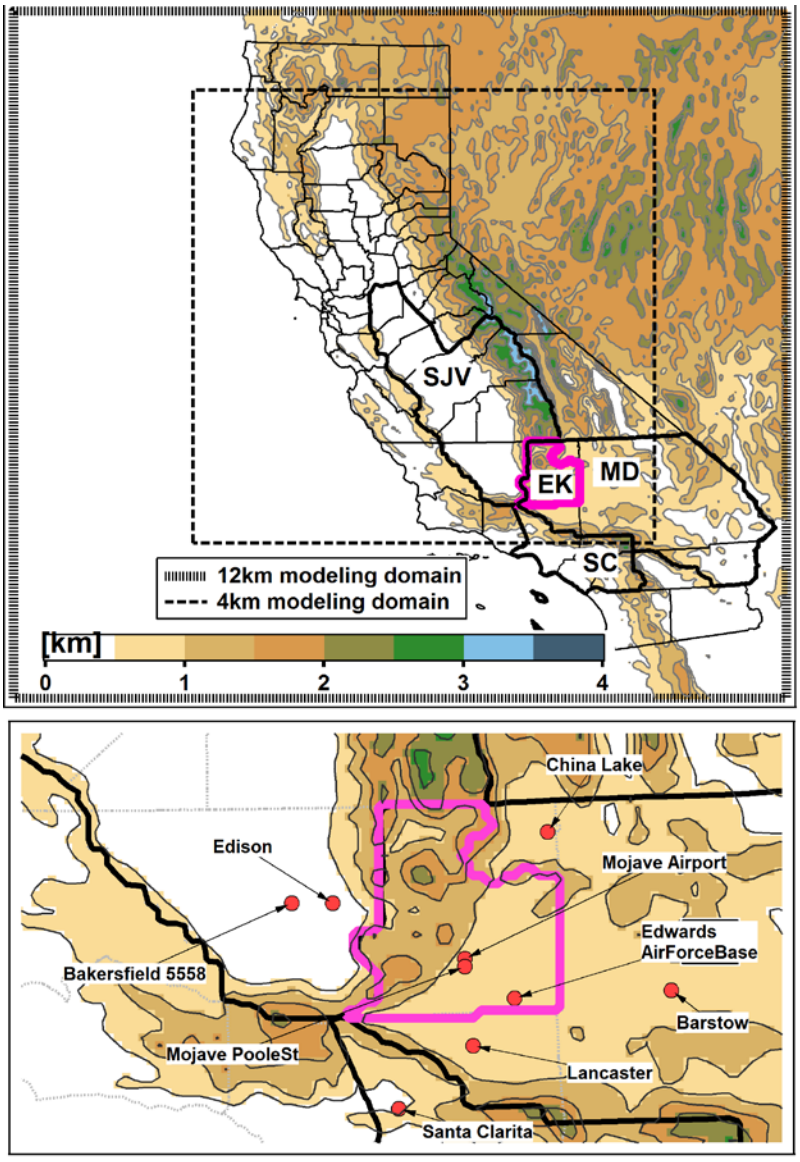

Figure 2. Trends in summer emissions of NOx and ROG (tons per day) between 2000 and 2020 in Eastern Kern, Western Kern and Los Angeles Counties. Anthropogenic emissions estimates are from the California Emission Projection Model (CEPAM) 2019 Ozone SIP Baseline Projection Version 1.04 with 2017 base year. 2018 biogenic ROG emissions are from MEGAN 3.0 biogenic model calculations. Note that emissions are represented on a log scale, which can mask small changes in the emissions.

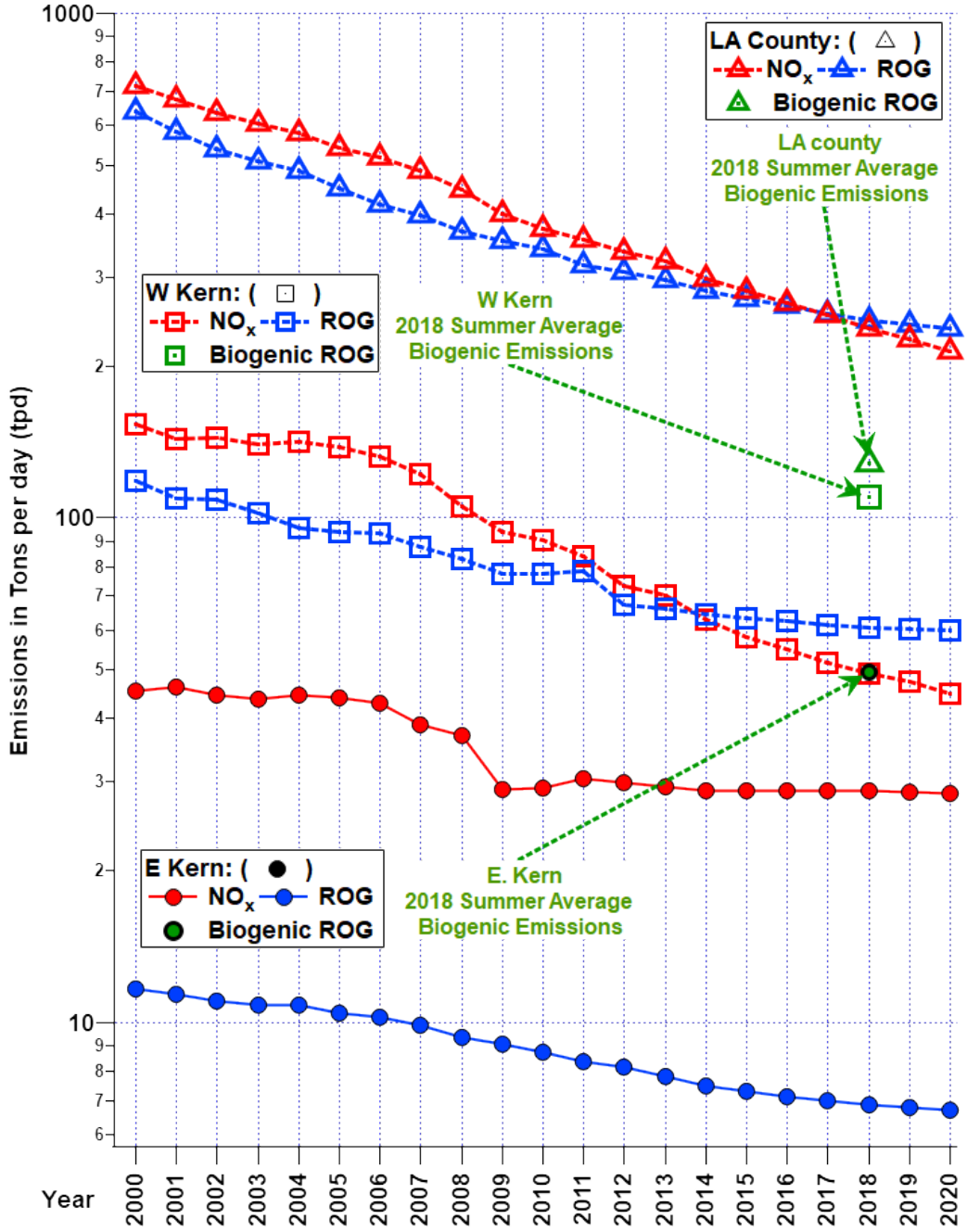

Figure 3. Trends in Eastern Kern's Maximum Daily Average 8-hour Ozone Design Value (ppb) and 70 ppb 8-hour Ozone NAAQS exceedance days between 2000 and 2020.

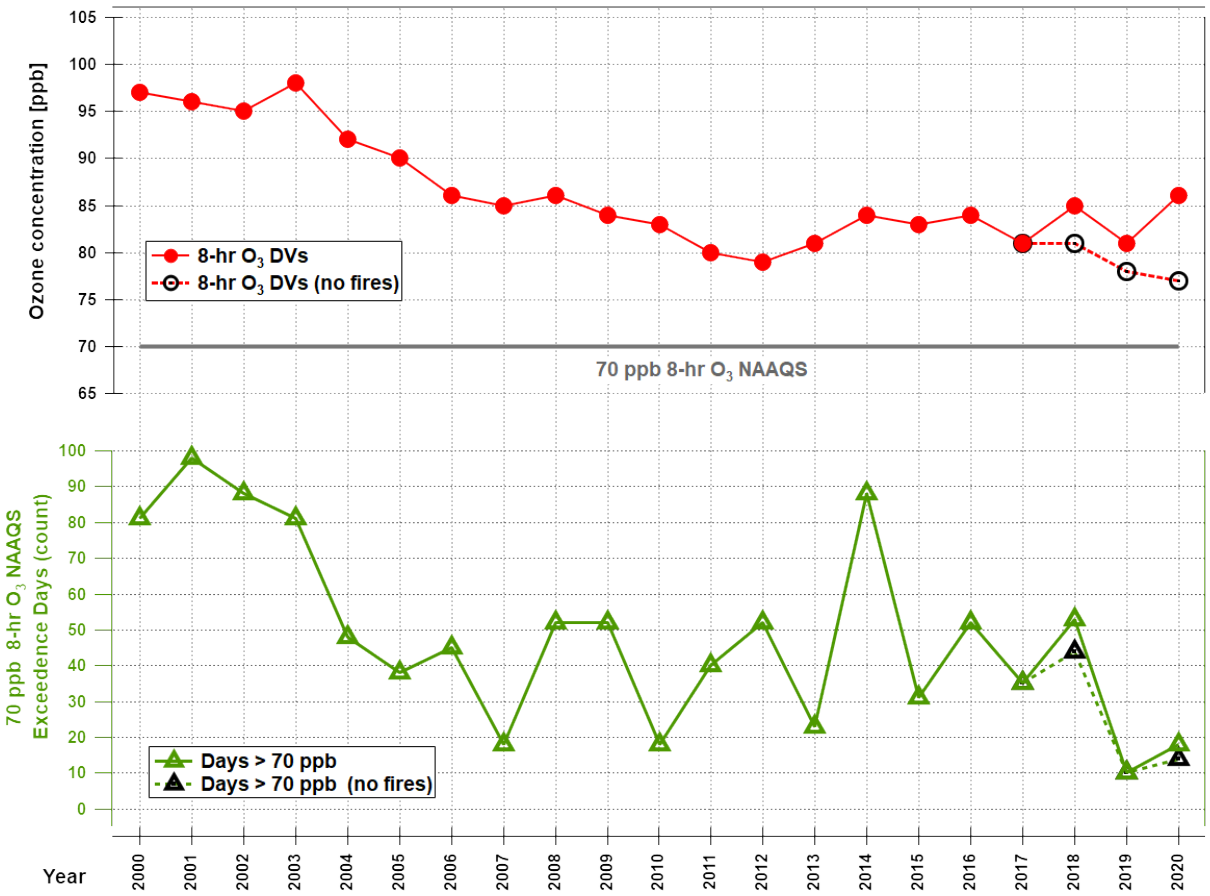

The EKNA is classified as severe nonattainment for the 2008 75 ppb O_3 standard and 2015 70 ppb O_3 standard, which means it has an attainment year of 2026 for the 75 ppb O_3 standard and an attainment year of 2032 for the 70 ppb O_3 standard. The remainder of this document serves as the modeling protocol and attainment demonstration for EKNA's 2022 Plan for both the 2008 75 ppb and 2015 70 ppb 8-hour ozone standards, which utilizes a base and reference year of 2018 and demonstrates attainment of the standard in 2026 (75 ppb) and 2032 (70 pbb).

II. Methodology

U.S. EPA modeling guidance (U.S. EPA, 2018) outlines the approach for utilizing regional chemical transport models (CTMs) to predict future attainment of the 2015 (70 ppb) 8-hour ozone standard. This model attainment demonstration requires that CTMs be used in a relative sense, where the relative change in ozone to a given set of emission reductions (i.e., predicted change in future anthropogenic emissions) is modeled, and then used to predict how current/present-day ozone levels would change under the future emissions scenario.

The starting point for the attainment demonstration is the observational based design value (DV), which is used to determine compliance with the ozone standards. The DV for a specific monitor and year represents the three-year average of the annual 4th highest 8-hour ozone mixing ratio observed at the monitor. For example, the 8-hour O_3 DV for 2018 is the average of the observed 4th highest 8-hour O_3 mixing ratio from 2016, 2017, and 2018 (Table 1). The U.S. EPA recommends using an average of three DVs to better account for the year-to-year variability in ozone levels due to meteorology. This average DV is called the weighted DV (in the context of this SIP document, the weighted DV will also be referred to as the reference year DV or DV_R). Since 2018 represents the reference year for projecting DVs to the future, site-specific DVs should be calculated for the three-year periods ending in 2018, 2019, and 2020, and then these three DVs are averaged. However, 2020 was an atypical year with large societal changes in response to the COVID19 pandemic and is not suitable for use in the DV_R calculation. To remove the impact from 2020 observations, we utilize an alternative methodology for calculating the average DVs by excluding year 2020. In this method, the 8-hour O_3 DV for 2020 was replaced by the two-year average of the 4th highest 8-hour O_3 concentrations from 2018 and 2019. Table 1 illustrates the observational data from each year that goes into the average DV_R and Equation 1 shows how the DV_R is calculated.

Table 1. Data from each year that are utilized in the Design Value calculation for a specific year (DV Year), and the yearly weighting of data for the average Design Value calculation (or DV_R).

DV Year	Years Averaged for the Design Value (4th highest observed 8-hr O_3)			
2018	2016	2017	2018	
2019		2017	2018	2019
2020			2018	2019

$$DV_R = \frac{DV_{2018} + DV_{2019} + \frac{4th\ highest\ MDA8\ O_3\ (2018+2019)}{2}}{3} \quad (1)$$

Table 2 lists the 8-hour design values for the Mojave monitoring site in the EKNA that are utilized in this model attainment demonstration. The 2018 ozone average baseline design value at this site is 82.7.

Table 2. Year-specific 8-hour ozone design values for 2018, 2019 and 2020, and the average baseline design value (DV_R, represented as the average of three design values) for 2018 at the Mojave site located in the EKNA. The 2020 DV is the two-year average of the 4th highest 8-hour O_3 concentrations from 2018 and 2019.

Site (County, Air Basin)	2018 DV (ppb)	2019 DV (ppb)	2020 DV (ppb)	2018-2020 Average DV (ppb)
Mojave-923PooleSt (Kern, MDAB)	85	81	82	82.7

Projecting the reference DVs to the future requires three photochemical model simulations, described below:

1. Base Year Simulation

The base year simulation for 2018 is used to assess model performance (i.e., to ensure that the model is reasonably able to reproduce the observed ozone mixing ratios). Since this simulation will be used to assess model performance, it is essential to include as much day-specific detail as possible in the emissions inventory, including, but not limited to hourly adjustments to the motor vehicle and biogenic inventories based on local meteorological conditions, known wildfire and agricultural burning events, and any exceptional events such as refinery fires.

2. Reference Year Simulation

The reference year simulation was identical to the base year simulation, except that certain emissions events which are either random and/or cannot be projected to the future are removed from the emissions inventory. For 2018, the only difference between the base and reference year simulations was that wildfires were excluded from the reference year simulation.

3. Future Year Simulation

The future year simulation (2026 or 2032) was identical to the reference year simulation, except that the projected future year anthropogenic emission levels were used rather than the reference year emission levels. All other model inputs (e.g., meteorology, chemical boundary conditions, biogenic emissions, and calendar for day-of-week specifications in the inventory) are the same as those used in the reference year simulation.

Projecting the reference DVs to the future is done by first calculating the fractional change in ozone between the modeled future and reference years for each monitor location. These ratios, called “relative response factors” or RRFs, are calculated based on the ratio of modeled future year ozone to the corresponding modeled reference year ozone (Equation 2).

$$\text{RRF} = \frac{\frac{1}{N}\sum_{d=1}^{N}(MDA8\ O_3)_{future}^{d}}{\frac{1}{N}\sum_{d=1}^{N}(MDA8\ O_3)_{reference}^{d}} \quad (2)$$

Where, MDA8 O_3 refers to the maximum daily average 8-hour ozone, d refers to the day (chosen from the reference year), and N is the total number of days used in the RRF calculation. These MDA8 ozone values are based on the maximum simulated ozone within a 3x3 array of cells surrounding the monitor (Figure 4). Not all modeled days are used to calculate the average MDA8 ozone from the reference and future year simulations. The form of the 8-hour ozone NAAQS is such that it is focused on the days with the highest mixing ratios in any ozone season (i.e., the 4th highest MDA8 ozone). Therefore, the modeled days used in the RRF calculation also reflect days with the highest ozone levels. As a result, the current U.S. EPA modeling guidance (U.S. EPA, 2018) recommends using the 10 days with the highest modeled MDA8 ozone at each monitor location, where the 10 days are chosen from the reference year simulation and then the same corresponding days are selected from the future year simulation. Since the relative sensitivity to emissions changes (in both the model and real world) can vary from day-to-day due to meteorology and emissions (e.g., temperature dependent emissions or day-of-week variability) using the top 10 days ensures that the calculated RRF is not overly sensitive to any single day. Note that the MDA8 ozone from the reference and future year simulations are paired in both time (the same days are selected from each simulation) and space (the location of the peak MDA8 ozone within the 3x3 array of grid cells surrounding the monitor is selected from the reference year simulation and the same location is used when selecting the corresponding data from the future year simulation).

Figure 4. Example showing how the location of the MDA8 ozone for the top ten days in the reference and future years are chosen.

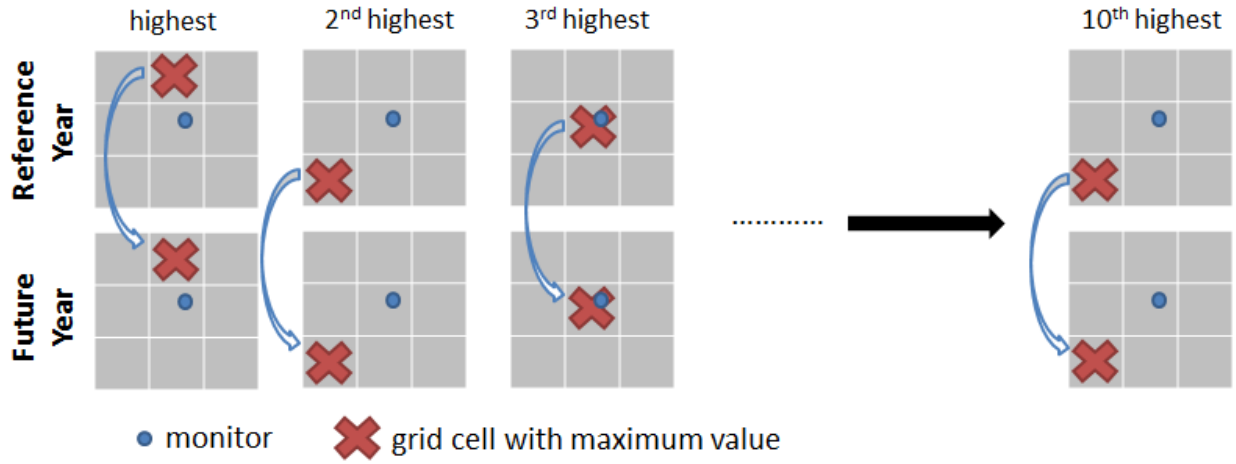

When choosing the top 10 days, the U.S. EPA recommends beginning with all days in which the simulated reference year MDA8 ozone is >= 60 ppb and then calculating RRFs based on the 10 days with the highest ozone in the reference simulation. If there are fewer than 10 days with MDA8 ozone >= 60 ppb then all days >= 60 ppb are used in the RRF calculation, as long as

there are at least 5 days used in the calculation. If there are fewer than 5 days >= 60 ppb, an RRF cannot be calculated for that monitor. To ensure that only modeled days which are consistent with the observed ozone levels are used in the RRF calculation, the modeled days are further restricted to days in which the reference MDA8 ozone is within ± 20% of the observed value at the monitor location.

Future year DVs at each monitor are then calculated by multiplying the corresponding reference year DV by the site-specific RRF.

$$DV_F = DV_R \times RRF \quad (3)$$

where, DV_F is the future year design value, DV_R is the reference year design value, and RRF is the site-specific RRF from Equation 2. The resulting future year DVs are then compared to the 8-hour ozone NAAQS to demonstrate whether attainment will be reached under the emissions scenario utilized in the future year modeling. A monitor is considered to be in attainment of the 8-hour ozone standard if the estimated future year DV does not exceed the level of the standard.

A. Meteorological Modeling

California's proximity to the ocean, complex terrain, and diverse climate represents a unique challenge for reproducing meteorological fields that adequately represent the synoptic and mesoscale features of the regional meteorology. In summertime, the majority of the storm tracks are far to the north of the state and a semi-permanent Pacific high pressure system typically sits off the California coast. Interactions between this eastern Pacific subtropical high-pressure system and the thermal low-pressure further inland over the Central Valley or South Coast lead to conditions conducive to pollution buildup over large portions of the state (Bao et al., 2008; Fosberg et al., 1966).

The state-of-the-science Weather Research and Forecasting (WRF) prognostic model (Skamarock, et al. 2008) version 4.2.1 was employed in the modeling. Its domain consisted of three nested Lambert projection grids of 36 km (D01), 12 km (D02), and 4 km (D03) uniform horizontal grid spacing as shown in Figure 5. The 4 km innermost domain has 427x427 grid points and spans 1748 km in the east-west and the north-south directions. All three domains utilized 30 vertical sigma layers with the lowest layer extending to 30 m above the surface (Table 3). The North America Regional Reanalysis (NARR) fields, enhanced with surface and upper-air observations, were used for initial and boundary conditions as well as Four Dimension Data Assimilation (FDDA) on the outermost (36 km) domain. The horizontal spatial resolution of the NARR data is 32 km. The major physics options for each domain are listed in Table 4, which include the Yon-Sei University (YSU) planetary boundary layer (PBL) scheme, Kain-Fritsch cumulus parameterization for the outer two domains, and 5-layer thermal diffusion land-surface option.

Figure 5. WRF modeling domains (D01 36 km; D02 12 km; and D03 4 km).

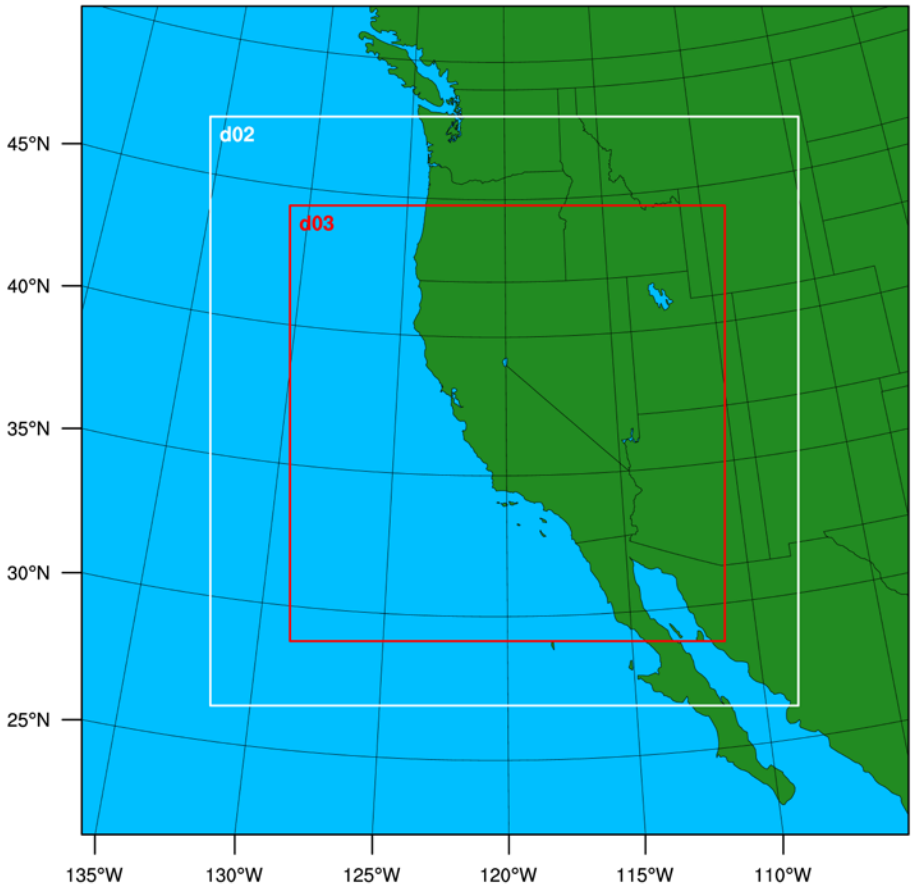

Table 3. WRF vertical layer structure.

Layer Number	Height (m)	Layer Thickness (m)	Layer Number	Height (m)	Layer Thickness (m)
30	16082	1192	15	2262	403
29	14890	1134	14	1859	334
28	13756	1081	13	1525	279
27	12675	1032	12	1246	233
26	11643	996	11	1013	194
25	10647	970	10	819	162
24	9677	959	9	657	135
23	8719	961	8	522	113
22	7757	978	7	409	94
21	6779	993	6	315	79
20	5786	967	5	236	66
19	4819	815	4	170	55
18	4004	685	3	115	46
17	3319	575	2	69	38
16	2744	482	1	31	31

To prevent any large deviations from the reanalysis data, analysis nudging was applied to the outermost domain (D01) above the planetary boundary layer (PBL) for moisture and above 2 km for wind and temperature. No nudging was used on the two inner domains to allow the model physics to work fully without externally imposed forcing. Boundary conditions on the outermost domain were updated every 6 hours, while WRF was reinitialized every 6 days with one day overlap, where the first day after being reinitialized was discarded as model spin-up. The Meteorology-Chemistry Interface Processor (MCIP) version 5.1 was used to process the 12 km (D02) and 4 km (D03) WRF output for use in the CTM simulations.

Table 4. WRF Physics options.

Physics Option	D01 (36 km)	D02 (12 km)	D03 (4 km)
Microphysics	WSM 6-class	WSM 6-class	WSM 6-class
Longwave Radiation	RRTM	RRTM	RRTM
Shortwave Radiation	Dudhia	Dudhia	Dudhia
Surface Layer	Revised MM5 Monin-Obukhov	Revised MM5 Monin-Obukhov	Revised MM5 Monin-Obukhov
Land Surface	5-layer Thermal Diffusion	5-layer Thermal Diffusion	5-layer Thermal Diffusion
Planetary Boundary Layer	YSU	YSU	YSU
Cumulus Parameterization	Kain-Fritsch Scheme	Kain-Fritsch Scheme	No

B. Emissions

The anthropogenic emissions inventory used in this modeling was based on the California Emissions Projection Analysis Model (CEPAM) v1.03 augmented with updates consistent with CEPAM v1.04 for select source categories. These sources are described in *http://outapp.arb.ca.gov/cefs/2019ozsip/CEPAM2019_key_updates_chron.pdf* under version "March 29, 2022 Release of Version 1.04 Planning Projections", except for emissions from Ocean Going Vessels (OGV). For a detailed description of the anthropogenic emissions inventory, updates to the inventory, and how it was processed from the planning totals to a gridded inventory for modeling, see the Modeling Emissions Inventory Appendix.

Table 5 summarizes the 2018, 2026 and 2032 EKNA anthropogenic emissions. Overall, anthropogenic NOx emissions in CEPAMv1.04 were projected to decrease by ~13.6% (from 20.5 tpd to 17.8 tpd) and 15% (20.5 tpd to 17.5 tpd) respectively in 2026 and 2032 when compared to 2018 levels with bulk of the reductions coming from on-road mobile sources. In contrast, anthropogenic ROG was projected to decrease by ~9.5% (from 7.7 tpd to 7.0 tpd) and 12% (from 7.7 tpd to 6.8 tpd) respectively in 2026 and 2032 when compared to the 2018 levels with the bulk of those reductions coming from all mobile sources including on-road and other

mobile sources. CEPAMv1.04 emissions for 2026 and 2032 reflect emission reductions from CARB's Heavy-Duty Vehicle Inspection and Maintenance (HD I/M) Program. The right two columns in Table 5 show the 2032 emissions after further incorporating CARB commitments from the State SIP Strategy, which are estimated at ~1.8 and 0.3 tpd additional reductions to the 2032 NO_x and ROG emission levels, respectively. Details on these rules/adjustments can be found in the Modeling Emissions Inventory Appendix.

Table 5. EKNA Summer Planning Emissions for 2018, 2026, and 2032 (tons/day).

	CEPAM1.04						With CARB Commitments	
Source Category	2018 NOx (tpd)	2018 ROG (tpd)	2026 NOx (tpd)	2026 ROG (tpd)	2032 NOx (tpd)	2032 ROG (tpd)	2032 NOx (tpd)	2032 ROG (tpd)
Stationary	12.8	1.4	12.3	1.5	12.4	1.6	12.4	1.6
Area	0.1	1.2	0.1	1.2	0.1	1.3	0.1	1.3
On-road Mobile	3.7	1.2	1.4	0.7	1.0	0.6	0.8	0.5
Other Mobile	4.0	3.9	3.9	3.6	3.9	3.4	2.3	3.2
Total	20.5	7.7	17.8	7.0	17.5	6.8	15.7	6.5

* Note that rounding errors may result in emissions totals that do not exactly match the sum of the individual categories.

Biogenic emissions were generated using the Model of Emissions of Gases and Aerosols from Nature (MEGAN3.0) biogenics emissions model (*https://bai.ess.uci.edu/megan*). MEGAN3.0 incorporates a new pre-processor (MEGAN-EFP) for estimating biogenic emission factors based on available landcover and emissions data. The MEGAN3.0 default datasets for plant growth form, eco-type, and emissions were utilized. Leaf Area Index (LAI) for non-urban grid cells was based on the 8-day 500 m resolution MODIS Terra/Aqua combined product (MCD15A2H) for 2018 (*https://earthdata.nasa.gov/*). The LAI data was converted to LAIv, which represents the LAI for the vegetated fraction within each grid cell, by dividing the gridded MODIS LAI values by the Maximum Green Vegetation Fraction for each grid cell (*https://archive.usgs.gov/archive/sites/landcover.usgs.gov/green_veg.html*). The MODIS LAI product does not provide information on LAI in urban regions, so urban LAIv was estimated from the US Forest Service's Forest Inventory and Analysis urban tree plot data, processed through the i-Tree v6 software (*https://www.itreetools.org/tools/i-tree-eco*). Hourly meteorology for MEGAN was provided by the 4 km WRF simulation described above, and all stress factor adjustments were turned off.

Monthly biogenic ROG totals for 2018 within the EKNA are shown in Figure 6 (note that the same biogenic emissions were used in the 2018, 2026 and 2032 modeling). Throughout the summer, biogenic ROG emissions ranged from ~25 tpd in May to 95 tpd in July and ~70 tpd in August, with the difference in emissions primarily due to monthly differences in temperature, solar radiation, and leaf area. In addition to biogenic ROG emissions, the MEGAN model also estimates NOx emissions from soils using the Yienger and Levy scheme (Yienger and Levy, 1995) that accounts for natural emissions from soils as well as enhanced emissions from managed crop lands. Figure 7 shows the monthly average soil NOx emissions for 2018 from MEGAN. Soil NOx emissions are highest during summer months where the emissions peak at 1.1 tpd in July.

Figure 6. Monthly average biogenic ROG emissions for 2018 in the EKNA.

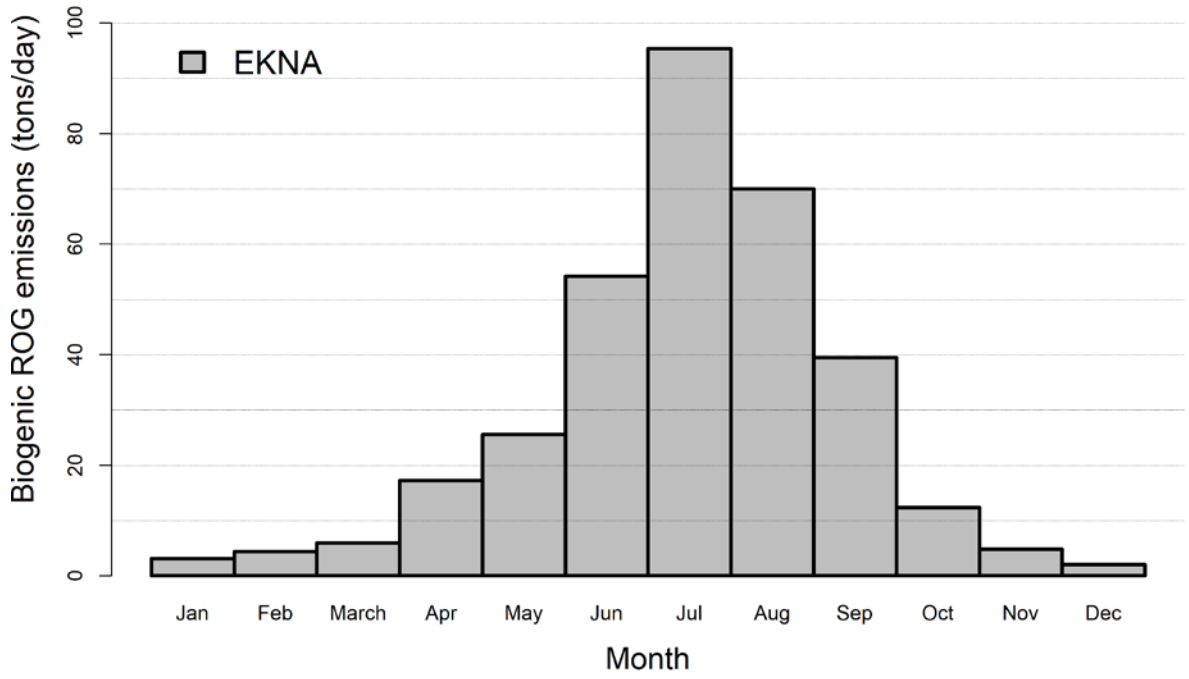

0

Figure 7. Monthly average soil NOx emissions for 2018 in the EKNA

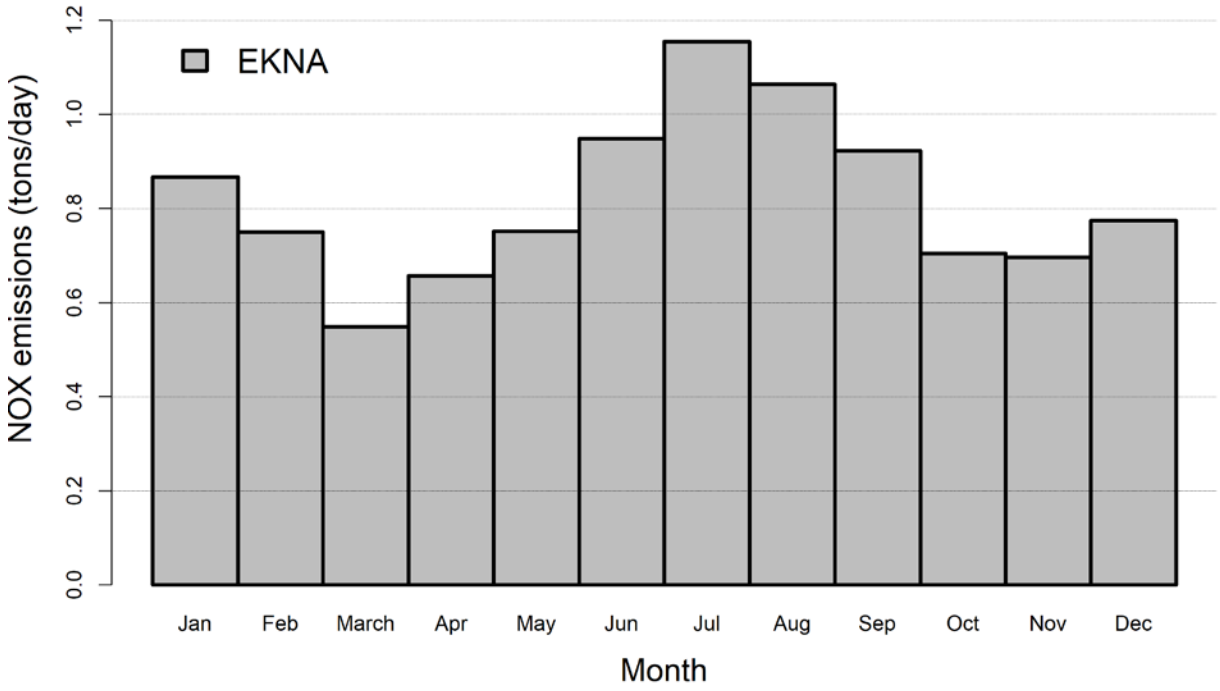

C. Air Quality Modeling

Figure 1 shows the Community Multiscale Air Quality (CMAQ) modeling domains used in this work. The larger domain covering all of California has a horizontal grid size resolution of 12 km with 107x97 lateral grid cells for each vertical layer and extends from the Pacific Ocean in the west to Eastern Nevada in the east and runs from the U.S.-Mexico border in the south to the California-Oregon border in the north. The smaller nested domain covering the Central valley region, including the San Joaquin Valley, Sacramento Valley, Mountain Counties air basins and the EKNA, has a finer scale 4 km grid resolution and includes 192x192 lateral grid cells. The 12 km and 4 km domains are based on a Lambert Conformal Conic projection with reference longitude at -120.5°W, reference latitude at 37°N, and two standard parallels at 30°N and 60°N, which is consistent with WRF domain settings. The CMAQ vertical layer structure is based on the WRF sigma-pressure coordinates and the exact layer structure used can be found in Table 3. The original 30 vertical layers from WRF were used for the CMAQ simulations, extending from the surface to 100 mb such that the majority of the vertical layers fall within the planetary boundary layer.

The CTM utilized in the modeling is the CMAQ model version 5.2.1 (U.S. EPA, 2018). CMAQ is the U.S. EPA's open-source regional air quality model, which is widely used in the regulatory and scientific communities, and represents the current state-of-the-science. CMAQ has been utilized for studying ozone and $PM_{2.5}$ formation in California for over a decade (e.g., Cai et al., 2016, 2019; Jin et al., 2008, 2010; Kelly et al., 2010, 2014; Livingstone et al., 2009; Pun et al., 2009; Tonse et al., 2008; Vijayaraghavan et al., 2006; Zhang et al., 2010), and has been the

primary CTM used in California SIPs since 2008 (SJV, 2008), having been used in over a dozen ozone and $PM_{2.5}$ SIPs (Eastern Kern, 2017; Imperial, 2017, 2018; Sacramento, 2017; SJV, 2012, 2013, 2016a,b, 2018; South Coast, 2012, 2016; Ventura, 2016; Western Mojave, 2016; Western Nevada, 2018).

The SAPRC07tic chemical mechanism (Carter, 2010a,b) was chosen to represent the gas-phase photochemistry in the atmosphere, along with the aero6 aerosol module for simulating aerosol dynamics and chemistry. Photolysis rates were calculated in-line to better represent changes in photolysis rates due to meteorological conditions and gaseous and particulate pollutant levels in the atmosphere.

Global chemical transport Community Atmosphere Model with Chemistry (CAM-Chem) coupled to the Community Earth System Model (CESM2) (Emmons, 2020; Lamarque et al., 2012) was developed by National Center for Atmospheric Research (NCAR) and used for simulations of global tropospheric and stratospheric atmospheric compositions. CAM-Chem modeling outputs have been widely used to provide chemical boundary conditions for various regional air quality models (Yan et al., 2021; He et al., 2018; Shahrokhishahraki et al., 2022; Wang et al., 2022). In this work, chemical boundary conditions for the outer 12-km domain were extracted from the CAM-Chem output based on vertical and horizontal setups of CMAQ meteorological inputs, and processed into CMAQ model ready format as well as mapped to CMAQ chemical species. The CAM-chem data for 2018 was obtained from the National Center for Atmospheric Research (*https://www.acom.ucar.edu/cam-chem/cam-chem.shtml*) *(Buchholz, 2019) and processed using the mozart2camx preprocessor version 3.2.3 (https://www.camx.com/download/support-software/)*. The same CAM-chem derived BCs for the 12 km outer domain were used for both base year, reference year and future year simulations. The inner 4 km domain simulations utilized BCs that were based on the output from the corresponding12 km domain simulations.

The extended ozone season (April – October) was simulated through parallel individual monthly simulations for the base year, reference year and future year. For each month, the CMAQ simulations included a seven-day spin-up period (i.e., the last seven days of the previous month) for the outer 12 km domain where initial conditions for the beginning day were set to the default initial conditions included with the CMAQ release. The 4 km inner domain simulations utilized a three-day spin-up period, where the initial conditions for the starting day were based on output from the corresponding day of the 12 km domain simulation. These spin-up periods were chosen based on previous testing, which showed that influence from the initial conditions was negligible after the seven- and three-day spin-up periods for the 12 km and 4 km simulations, respectively. Table 6 lists the CMAQ configuration and settings used in the modeling.

Table 6. CMAQ configuration and settings.

Process	Scheme
Advection	Yamo module for horizontal and WRF module for vertical
Horizontal diffusion	Multi-scale
Vertical diffusion	ACM2 (Asymmetric Convective Model version 2)
Gas-phase chemical mechanism	SAPRC version 07tc gas-phase mechanism with extended isoprene chemistry
Chemical solver	EBI (Euler Backward Iterative solver)
Aerosol module	Aero6 (the sixth generation CMAQ aerosol mechanism)
Cloud module	ACM_AE6 (ACM cloud processor that uses the ACM methodology to compute convective mixing with heterogeneous chemistry for AERO6)
Photolysis rate	Phot/inline (calculating photolysis rates inline)

III. Results

A. Meteorological Model Evaluation

Simulated surface wind speed, temperature, and relative humidity from the 4 km domain were validated against hourly observations from 25 surface stations in the region (Figure 8). The observational data for the surface stations were obtained from the ARB archived meteorological database available at *http://www.arb.ca.gov/aqmis2/aqmis2.php*. Table 7 lists the monitoring stations and the meteorological parameters that are measured at each station, including wind speed and direction (wind), temperature at 2 meters (T2) above ground level (AGL) and relative humidity at 2 meters (RH2) AGL. Several quantitative performance metrics were used to compare hourly surface observations and modeled estimates: mean bias (MB), mean error (ME) and index of agreement (IOA) based on the recommendations from Simon et al. (2012). The model performance statistical metrics were calculated using the available data at all the sites. A summary of these statistics for the area is shown in Table 8.

The average hourly wind speed bias for April-October 2018 is relatively small at -0.07 m/s, while the average mean error is 0.48 m/s. The index of agreement for the wind speed in this period is 0.92. Temperature is biased low with an average bias of -0.72 K, while the IOA for temperature is 0.96. Consistent with the negative temperature bias, relative humidity has a positive bias of 12.9%. The distribution of daily mean bias and mean error for wind speed, temperature and relative humidity are shown in Figure 9. The spatial distributions of the mean bias and mean error of modeled surface wind, temperature and relative humidity are shown in

Figure 10. Observed vs. modeled scatter plots of hourly wind speed, temperature, and relative humidity are shown in Figure 11. These results are comparable to other WRF modeling efforts in California investigating ozone formation in Central California (e.g. Hu et al., 2012) and modeling analysis for the CalNex, CARES and Discover-AQ field studies (e.g. Fast et al., 2012; Baker et al., 2013; Kelly et al., 2014; Angevine et al., 2012; Chen et al., 2020). Detailed hourly time-series of surface temperature, relative humidity, wind speed, and wind direction can be found in the supplemental materials.

Table 7. Meteorological site location and parameter measured.

Site Number (Figure 8)	Site ID	Site Name	Parameter(s) Measured
1	5823	Delano #2	Wind, T2, RH2
2	3476	UHL	Wind
3	5729	Blackwells Corner	Wind, T2, RH2
4	5709	Shafter – USDA	Wind, T2, RH2
5	5791	Belridge	Wind, T2, RH2
6	2981	Shafter-Walker Street	Wind
7	2772	Oildale-3311 Manor Street	Wind
8	3146	Bakersfield-5558 Cali. Avenue	Wind
9	2312	Edison	Wind
10	3353	Jawbone	Wind
11	5771	Arvin-Edison	Wind, T2, RH2
12	2919	Maricopa-Stanislaus Street	Wind
13	3121	Mojave-923 Poole Street	Wind
14	5414	Lebec	Wind
15	3316	Poppy Park	Wind
16	3645	Saddleback Butte	Wind

Site Number (Figure 8)	Site ID	Site Name	Parameter(s) Measured
17	5834	Palmdale #4	Wind, T2, RH2
18	3326	Acton	Wind
19	3544	Del Valle	Wind
20	7220	Santa Clarita (CIMIS)	Wind, T2, RH2
21	3358	Saugus	Wind
22	3480	Mill Creek (ANF)	Wind
23	3502	Santa Clarita	Wind
24	3359	Camp 9	Wind
25	3329	Chilao	Wind

Figure 8. Meteorological monitoring sites utilized in the model evaluation for Eastern Kern. Numbers reflect the sites listed in Table 7.

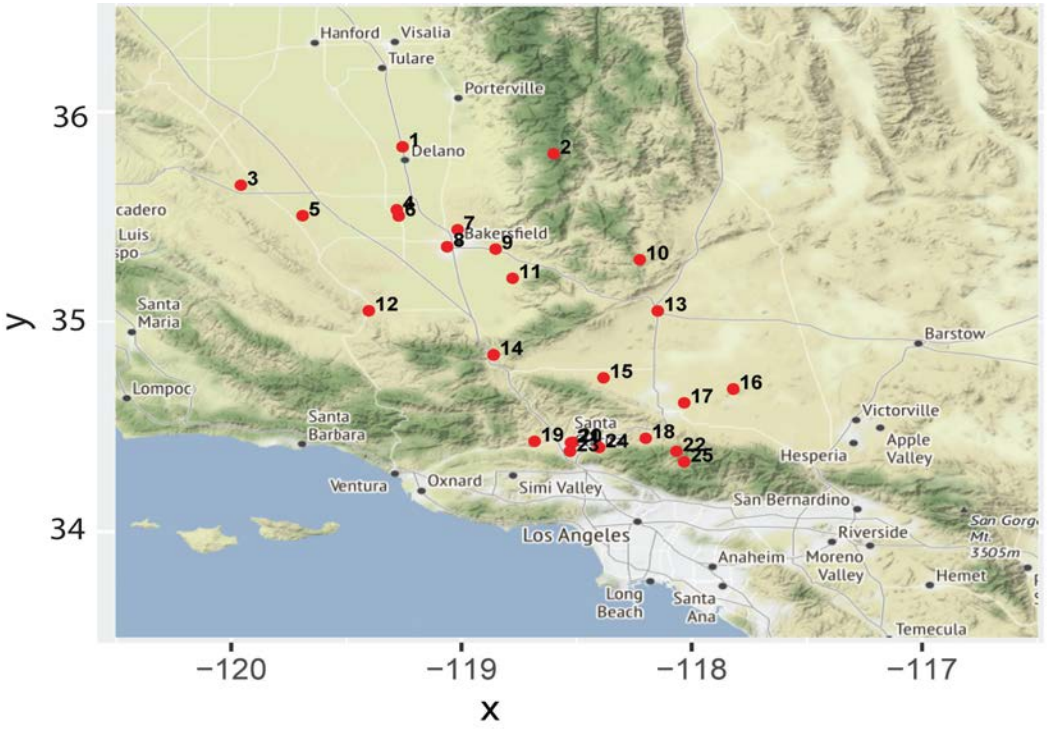

Table 8. Hourly surface wind speed, temperature and relative humidity statistics for April through October, 2018. IOA denotes index of agreement.

	Observed Mean	Modeled Mean	Mean Bias	Mean Error	IOA
Wind Speed (m/s)	3.10	3.03	-0.07	0.48	0.92
Temperature (K)	295.48	294.76	-0.72	2.17	0.96
Relative Humidity (%)	48.21	61.11	12.9	13.57	0.78

Figure 9. Distribution of daily mean bias (left) and mean error (right) from April –October 2018. Results are shown for wind speed (top), temperature (middle), and RH (bottom).

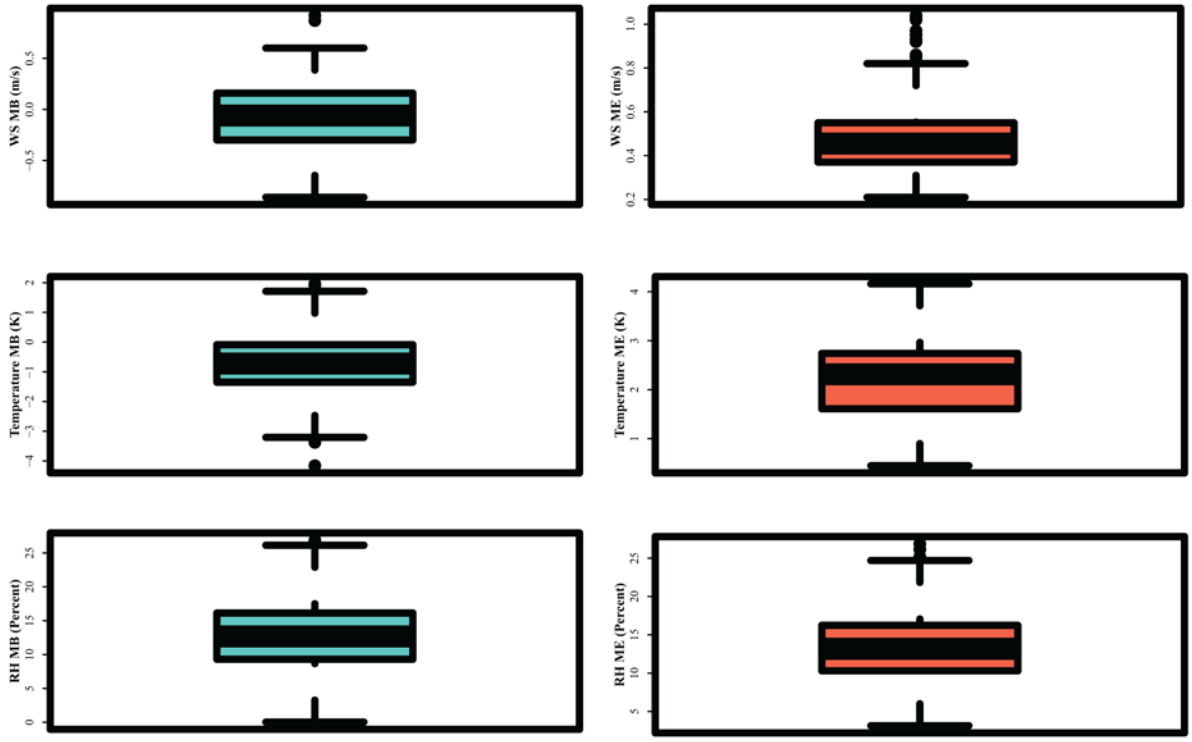

Figure 10. Spatial distribution of mean bias (left) and mean error (right) for April-October 2018. Results are shown for wind speed (top), temperature (middle), and RH (bottom).

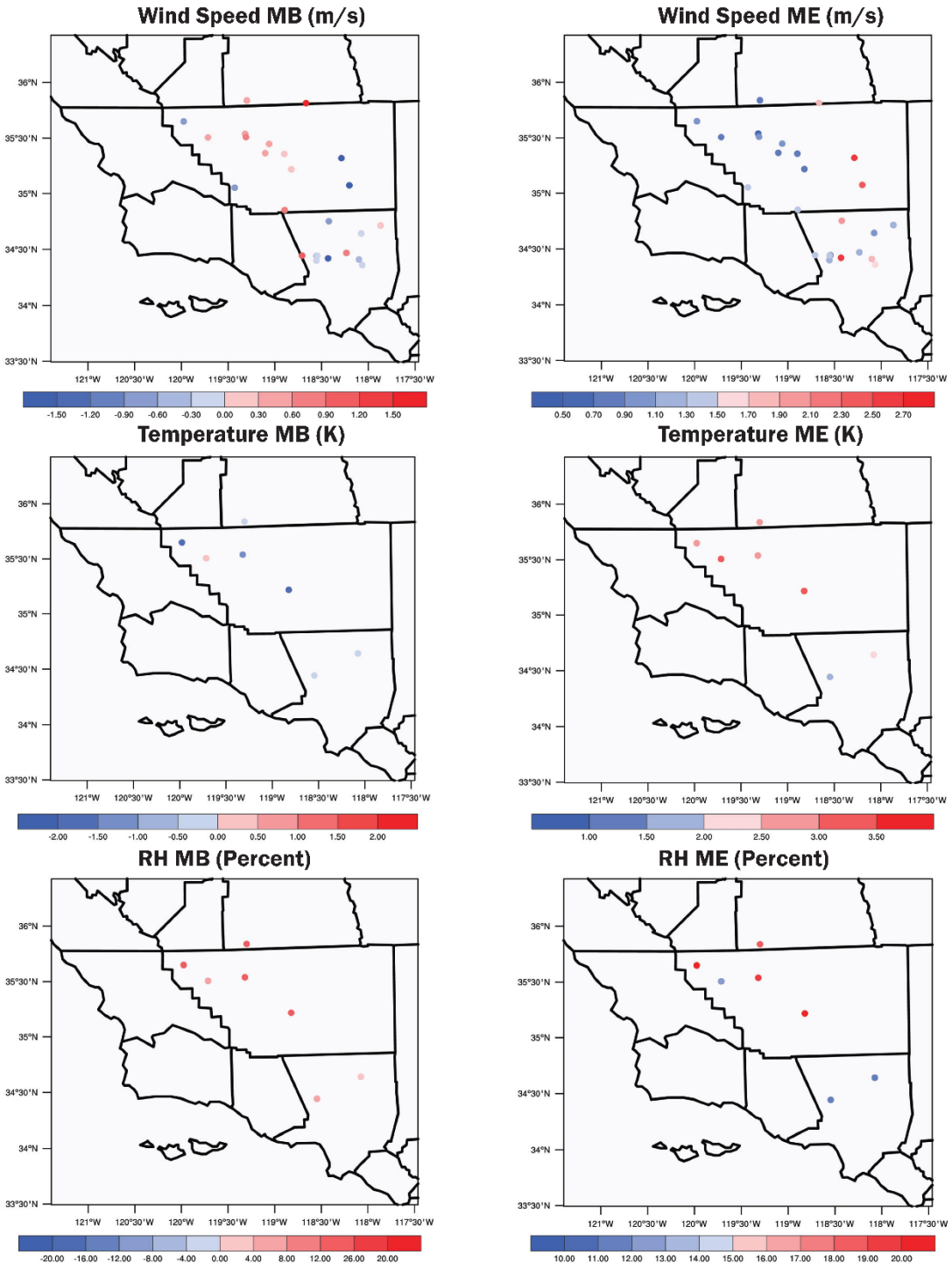

Figure 11. Comparison of modeled and observed hourly wind speed (left), 2-meter temperature (center), and relative humidity (right), April – October 2018.

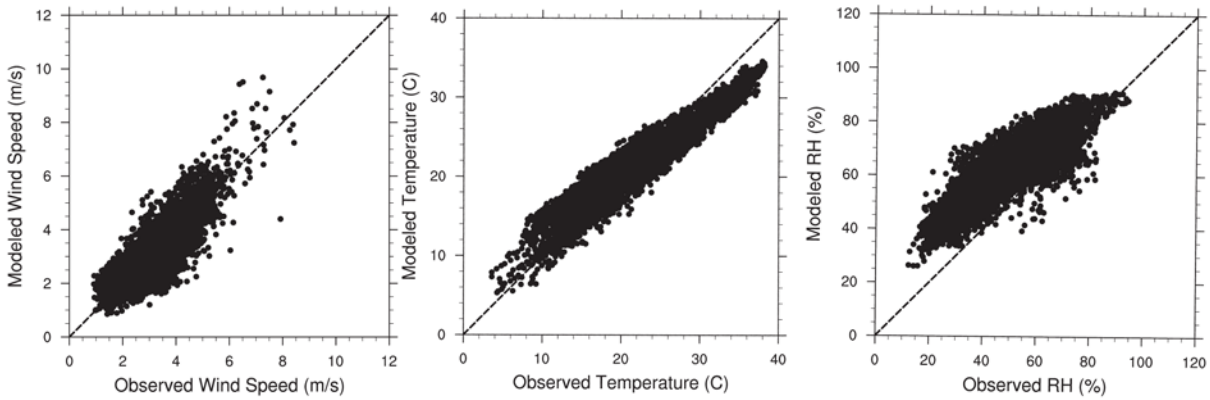

B. Phenomenological Evaluation

Conducting a detailed phenomenological evaluation for all modeled days can be resource intensive given that the entire ozone season (April – October) was modeled for the attainment demonstration. However, some insight and confidence that the model is able to reproduce the meteorological conditions leading to elevated ozone can be gained by investigating the meteorological conditions during peak ozone days within the EKNA in more detail.

Meteorological conditions that produced peak ozone levels in the area occurred on August 7, 2018, with a daily maximum 8-hour ozone mixing ratio of 94 ppb observed at the Mojave ozone monitoring site. The upper-air weather charts showed that a 500 mb high pressure system was observed over California. The pressure gradient of this system was weak and the daytime temperature at the Mojave monitor reached 97 ˚F.

Figure 12 shows the surface wind fields in the early afternoon (13:00 PST) and evening (20:00 PST) on August 7, 2018 with the observed and modeled values denoted by red and black arrows, respectively. Overall, modeled winds compare relatively well with the observed values, with winds during the early afternoon hours being influenced by up slope flows, while evening winds were impacted by down slope flows. The winds were stronger through the mountain passes such as Soledad Canyon between Santa Clarita and Palmdale and the Tehachapi pass, facilitating transport of pollutants from SoCAB and SJVAB into the EKNA.

Since RRF calculations in the model attainment test described previously are based on the top 10 peak ozone days, the modeled and measured winds in the area were examined further for the top 10 ozone days observed at the Mojave site in 2018. The ten highest maximum daily average 8-hour ozone mixing ratios observed at the Mojave site in 2018 occurred on August 7, August 9, August 4, July 29, July 30, July 31, August 8, August 6, August 10, June 20, respectively. Figure 13 shows the mean wind field (vector average) for the top 10 ozone days at 05:00 PST and 13:00 PST, respectively. Overall, the surface wind distribution indicates that the model is in general agreement with the observations and is able to capture many of the important features of the observed meteorological fields on those days when elevated ozone levels occurred.

Figure 12. Surface wind field at 13:00 PST (top) and 20:00 PST (bottom) on August 07, 2018. Modeled wind field is shown with black wind vectors, while observations are shown in red.

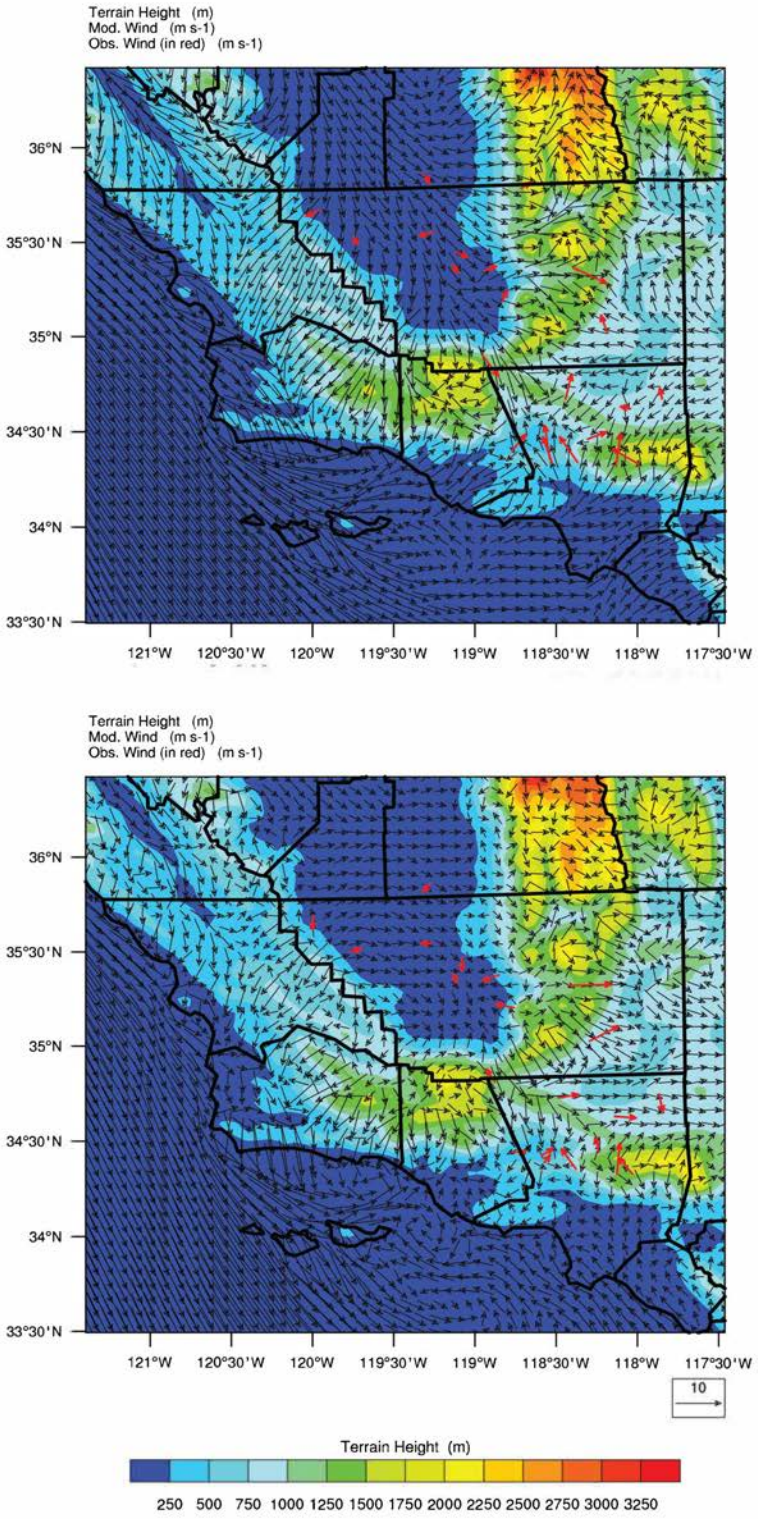

Figure 13. Average wind field at 5:00 PST (top) and 13:00 PST (bottom) for the top 10 observed ozone days at Mojave monitor in 2018. Modeled wind field is shown with black wind vectors, while observations are shown in red.

In addition, it is useful to examine the direction of predominant wind flow, through wind rose plots, on peak ozone days to ensure the same transport patterns from source to receptor observed in the atmosphere are also captured in the model. Figure 14 shows the observed and simulated wind speed frequency and direction at the Mojave site for the top 10 ozone days in 2018. From Figure 14, it is clear that the dominant wind flow pattern on peak ozone days is from the west/north-west. The model predicted higher occurrences of winds from the west/north-west, and lower occurrences of winds from the west and west/south-west compared to observations. Despite less variability in wind directions, the model was generally able to reproduce the predominant wind directions.

Figure 14. Observed (left) and modeled (right) wind roses at the Mojave site for the top 10 observed ozone days in 2018.

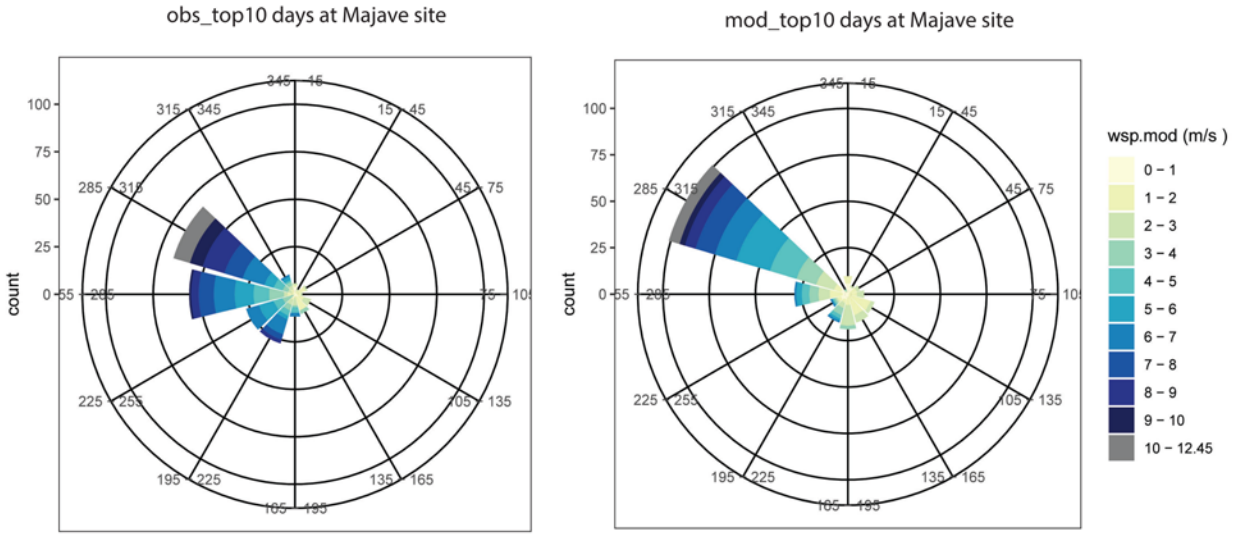

Figure 15 shows the 500 hPa geopotential height at 12:00 UTC and 00:00 UTC for the top 10 ozone days in 2018 at the Mojave site. These times were chosen to coincide with timing of the upper-air observations. In this figure, the North American Regional Reanalysis (NARR) data is used to represent the observations. The NARR dataset is a product of observational data assimilated into some of the NOAA model products for the purpose of producing a snapshot of the weather over North America at any given time. The 500 hPa geopotential height is a useful metric to evaluate, because most weather systems follow the winds at this level. It can be seen from Figure 15 that on average the 500 hPa geopotential height is ~5900 m above sea level and the modeled 500 hPa geopotential height closely matches the observed values.
Although a phenomenological evaluation of only a subset of peak ozone days does not necessarily mean the model performs equally well on all days, the fact that the model can adequately reproduce wind flows consistent with the ozone conceptual model, combined with reasonable performance statistics over the ozone season (Table 8), provides added confidence in the meteorological fields utilized for this attainment demonstration modeling.

Figure 15. Modeled and observed at 12:00 UTC (top) and 00:00 UTC (bottom) 500 hPa geopotential height for the top 10 observed ozone days in 2018.

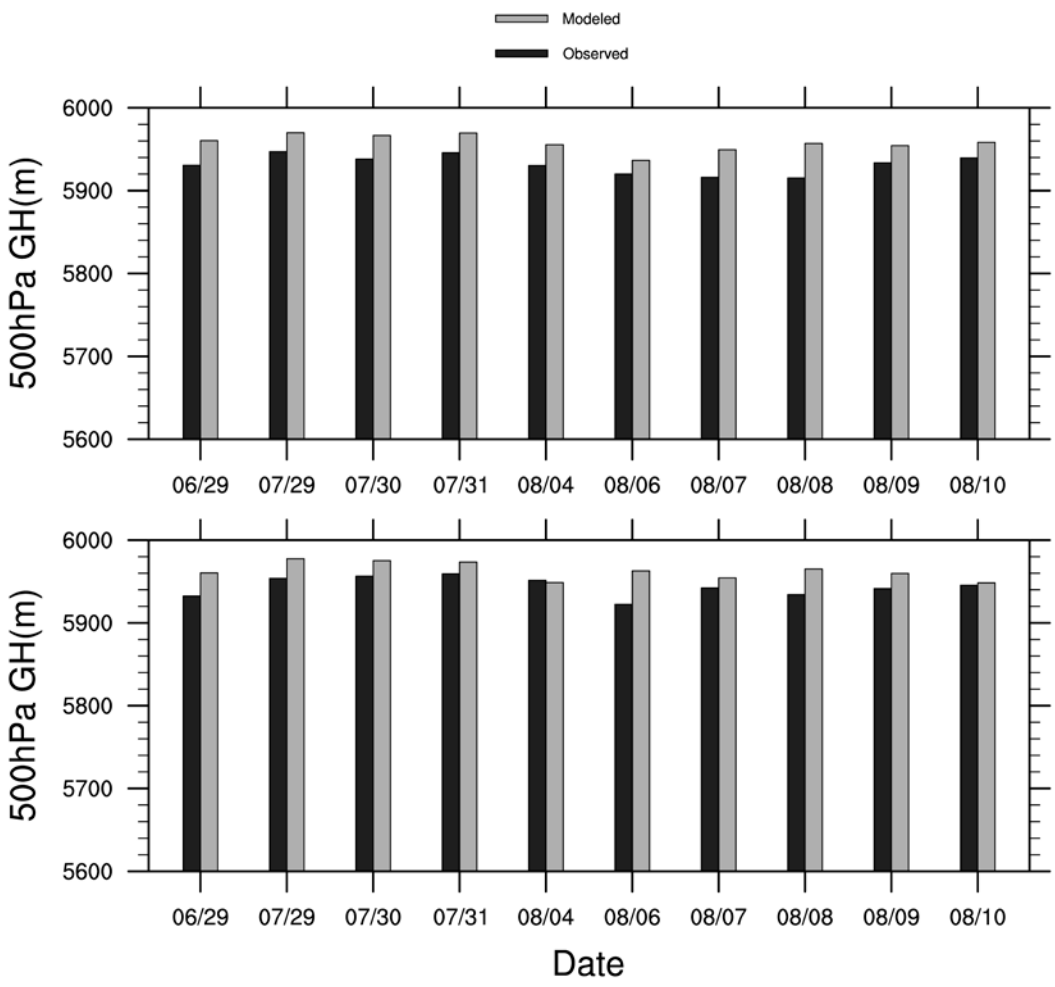

C. Air Quality Model Evaluation

Observed ozone data from CARB's Air Quality and Meteorological Information System (AQMIS) database (*www.arb.ca.gov/airqualitytoday/*) and Aerometric Data Analysis and Management (ADAM) database (*www.arb.ca.gov/adam/*) were used to evaluate the accuracy of the 4 km CMAQ modeling for ozone at the Mojave site in the EKNA. The U.S. EPA modeling guidance (U.S. EPA, 2018) recommends using the grid cell value where the monitor is located, to pair observations with simulated values in operational evaluation of model predictions. Since the future year design value calculations are based on simulated values near the monitor (i.e., the maximum simulated ozone within a 3x3 array of grid cells with the grid cell containing the monitor located at the center of the array), model performance was evaluated by comparing observations against the simulated values at the monitored grid cell as well as the peak grid cell within the 3x3 grid array centered on the monitor (i.e., the 3x3 maximum). While different cutoff criteria have be used in different model evaluation studies (Emery et al., 2017), U.S. EPA

suggests the days with simulated values > 60 ppb should receive higher priority in evaluation to give more attention to the model outputs that could potentially impact the outcome of the attainment test.

As recommended by U.S. EPA modeling guidance, a number of statistical metrics have been used to evaluate the model performance for ozone. These metrics include mean bias (MB), mean error (ME), mean fractional bias (MFB), mean fractional error (MFE), normalized mean bias (NMB), normalized mean error (NME), root mean square error (RMSE), and correlation coefficient (R^2). In addition, the following plots were used in evaluating the modeling with all available data: time-series plots comparing the predictions and observations, scatter plots for comparing the magnitude of the simulated and observed concentrations, as well as frequency distributions.

The model performance evaluation is presented for the Mojave site in the EKNA. Performance statistics for modeling scenarios with all valid data and only data above 60 ppb are reported separately for different ozone metrics including maximum daily average 8-hour ozone, maximum daily average 1-hour ozone, and hourly ozone (all hours of the day) for the monitored grid cell as well as the 3x3 maximum. Performance statistics for maximum daily average 8-hour ozone are shown in Table 9 and Table 10. Overall, when simulated data extracted at the grid cell are used for comparison with observations (as shown in Table 9), the model shows a bias of 0.41 ppb of maximum daily average 8-hour ozone in the EKNA. However, when only data greater than 60 ppb are used, model shows a negative bias of -3.49 ppb. Similarly, when the 3x3 maximum data is used for comparison, there is a positive bias in the model with all the valid data (1.74 ppb) and a negative bias with only data over 60 ppb (-2.15 ppb). This result indicates the model has a slight under-prediction of maximum daily average 8-hour ozone at high values in the EKNA. Similar statistics for maximum daily average 1-hour ozone and hourly ozone can be found in Table 11 to Table 13.

Model performance statistics within the range of values shown in Table 9 to Table 13 are consistent with previous studies in California and studies elsewhere in the U.S. Hu et al. (2012), simulated an ozone episode in central California (July 27 – August 2, 2000) using SAPRC07 chemical mechanism and found that a model bias of -10.8 ppb for maximum daily average 8-hour ozone with 60 ppb cutoff (compared to -3.49 ppb for EKNA in Table 9 of this work). Hu et al. also shows a model bias of -12.7 ppb for maximum daily average 1-hour ozone in Central California with 60 ppb cutoff (compared to -3.83 ppb in Table 11 of this work).

Similarly, Shearer et al. (2012) compared model performance in Central California during two episodes in 2000 (July 24 – 26 and July 31 – August 2) for two different chemical mechanisms and found that normalized bias for maximum daily average 8-hour ozone ranged from -7% to -14% with hourly peak ozone showing a range of -7% to -18%. These values are greater than the statistics found in this work, which were calculated as 0.65% for maximum daily average 8-hour ozone and -0.94% for maximum daily average 1-hour ozone. Jin et al. (2010) conducted a longer term simulation over Central California (summer 2000) and found a RMSE for maximum daily average 8-hour ozone of 14 ppb, which is greater than the 8.91 ppb found in this work. Jin et al. (2010) also showed an overall negative bias of -2 ppb, which is in the similar range of 0.41 ppb (1.74 ppb with 3x3 maximum values) found in this work. Zhu et al. (2019) shows hourly O_3

NMB of 8.2% and NME of 11.3% for July and August 2012 with 20ppb cutoff, both are similar to the NMB and NME shown in Table 13.

Table 9. Maximum daily average 8-hour ozone performance statistics in the EKNA for the 2018 ozone season (April - October). Maximum daily average 8-hour ozone with simulated data extracted at grid cell where the monitor is located.

Parameter	EKNA	EKNA with data over 60 ppb
Number of data points	212	130
Mean obs (ppb)	62.67	70.09
Mean Bias (ppb)	0.41	-3.49
Mean Error (ppb)	6.94	6.12
RMSE (ppb)	8.91	8.07
Mean Fractional Bias (%)	1.40	-5.20
Mean Fractional Error (%)	11.36	8.98
Normalized Mean Bias (%)	0.65	-4.98
Normalized Mean Error (%)	11.07	8.73
R-squared	0.42	0.28

Table 10. Maximum daily average 8-hour ozone performance statistics in the EKNA for the 2018 ozone season (April - October). Maximum daily average 8-hour ozone with simulated data extracted from the 3x3 grid cell array maximum centered at the monitor.

Parameter	EKNA	EKNA with data over 60 ppb
Number of data points	212	130
Mean obs (ppb)	62.67	70.09
Mean Bias (ppb)	1.74	-2.15
Mean Error (ppb)	7.14	5.91

Parameter	EKNA	EKNA with data over 60 ppb
RMSE (ppb)	9.14	7.73
Mean Fractional Bias (%)	3.51	-3.19
Mean Fractional Error (%)	11.63	8.58
Normalized Mean Bias (%)	2.78	-3.06
Normalized Mean Error (%)	11.39	8.44
R-squared	0.42	0.26

Table 11. Maximum daily average 1-hour ozone performance statistics in the EKNA for the 2018 ozone season (April - October). Maximum daily 1-hour ozone with simulated data extracted at grid cell where the monitor is located.

Parameter	EKNA	EKNA with data over 60 ppb
Number of data points	211	154
Mean obs (ppb)	67.90	73.90
Mean Bias (ppb)	-0.64	-3.83
Mean Error (ppb)	7.81	7.36
RMSE (ppb)	10.02	9.53
Mean Fractional Bias (%)	-0.17	-5.38
Mean Fractional Error (%)	11.81	10.28
Normalized Mean Bias (%)	-0.94	-5.18
Normalized Mean Error (%)	11.50	9.96
R-squared	0.45	0.36

Table 12. Daily maximum 1-hour ozone performance statistics in the EKNA for the 2018 ozone season (April - October). Daily Maximum 1-hour ozone with simulated data extracted from the 3x3 grid cell array maximum centered at the monitor.

Parameter	EKNA	EKNA with data over 60 ppb
Number of data points	211	154
Mean obs (ppb)	67.90	73.90
Mean Bias (ppb)	1.19	-1.89
Mean Error (ppb)	7.83	6.98
RMSE (ppb)	10.17	9.20
Mean Fractional Bias (%)	2.52	-2.63
Mean Fractional Error (%)	11.77	9.59
Normalized Mean Bias (%)	1.75	-2.56
Normalized Mean Error (%)	11.53	9.45
R-squared	0.44	0.33

Table 13. Hourly ozone performance statistics in the EKNA for the 2018 ozone season (April - October). Hourly ozone with simulated data extracted at grid cell where the monitor is located. Note that only statistics for the grid cell in which the monitor is located were calculated for hourly ozone.

Parameter	EKNA	EKNA with data over 60 ppb
Number of data points	4903	1949
Mean obs (ppb)	55.49	68.86
Mean Bias (ppb)	1.40	-5.93
Mean Error (ppb)	8.70	8.42
RMSE (ppb)	11.19	10.76

Parameter	EKNA	EKNA with data over 60 ppb
Mean Fractional Bias (%)	4.57	-9.34
Mean Fractional Error (%)	16.77	12.96
Normalized Mean Bias (%)	2.52	-8.61
Normalized Mean Error (%)	15.68	12.22
R-squared	0.39	0.14

Simon et al. (2012) conducted a review of photochemical model performance statistics published between 2006 and 2012 for North America (from 69 peer-reviewed articles). In Figure 16, the statistical evaluation of this model attainment demonstration is compared to the model performance summary presented in Simon et al. (2012) by overlaying various summary statistics onto the Simon et al. (2012) model performance summary. Note that the box-and-whisker plot (colored in black) shown in Figure 16 is reproduced using data from Figure 4 of Simon et al. (2012). The red dot and blue triangle in each of the panels in Figure 16 denote the model performance statistics from the current modeling work, calculated using the simulated monitor grid cell and the 3x3 maximum, respectively.

Figure 16. Comparison of various statistical metrics from the model attainment demonstration modeling to the range of statistics from the 69 peer-reviewed studies summarized in Simon et al (2012). (MDA denotes Maximum Daily Average). Red circular markers show statistics calculated from modeled ozone at the monitor location, while blue triangular markers show statistics calculate from the maximum ozone in the 3x3 array of grid cells surrounding the monitor.

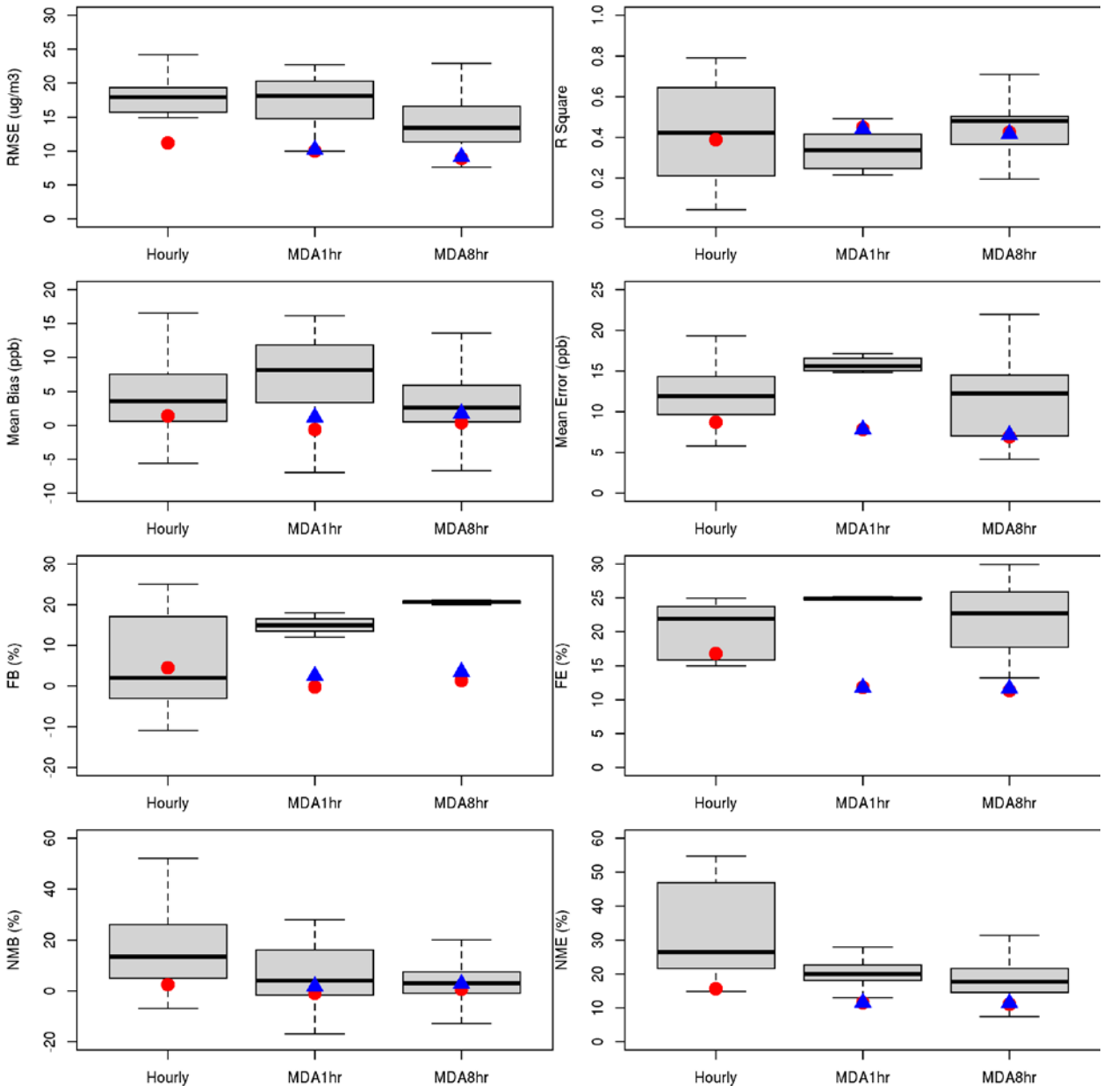

Figure 16 clearly shows that the model performance statistical metrics for hourly, maximum daily average 8-hour and maximum daily 1-hour ozone from this work are consistent with previous modeling studies reported in the scientific literature, and in most cases are better than those statistics. In particular, the Simon et al. (2012) study found that mean bias for maximum

daily average 8-hour ozone ranged from approximately -7 ppb to 13 ppb, while mean error ranged from around 4 ppb to 22 ppb, and RMSE varied from approximately 8 ppb to 23 ppb; all of which are similar in magnitude to the statistics presented in Table 9 and Table 10.

Figure 17. Average MDA8 ozone for the top 10 ozone days in 2018 from the model simulations overlaid with observation data (SJV and SoCAB sites marked as circle, Mojave-923PooleSt marked as triangle), where the top 10 days from the observations were chosen based on the Mojave-923PooleSt site.

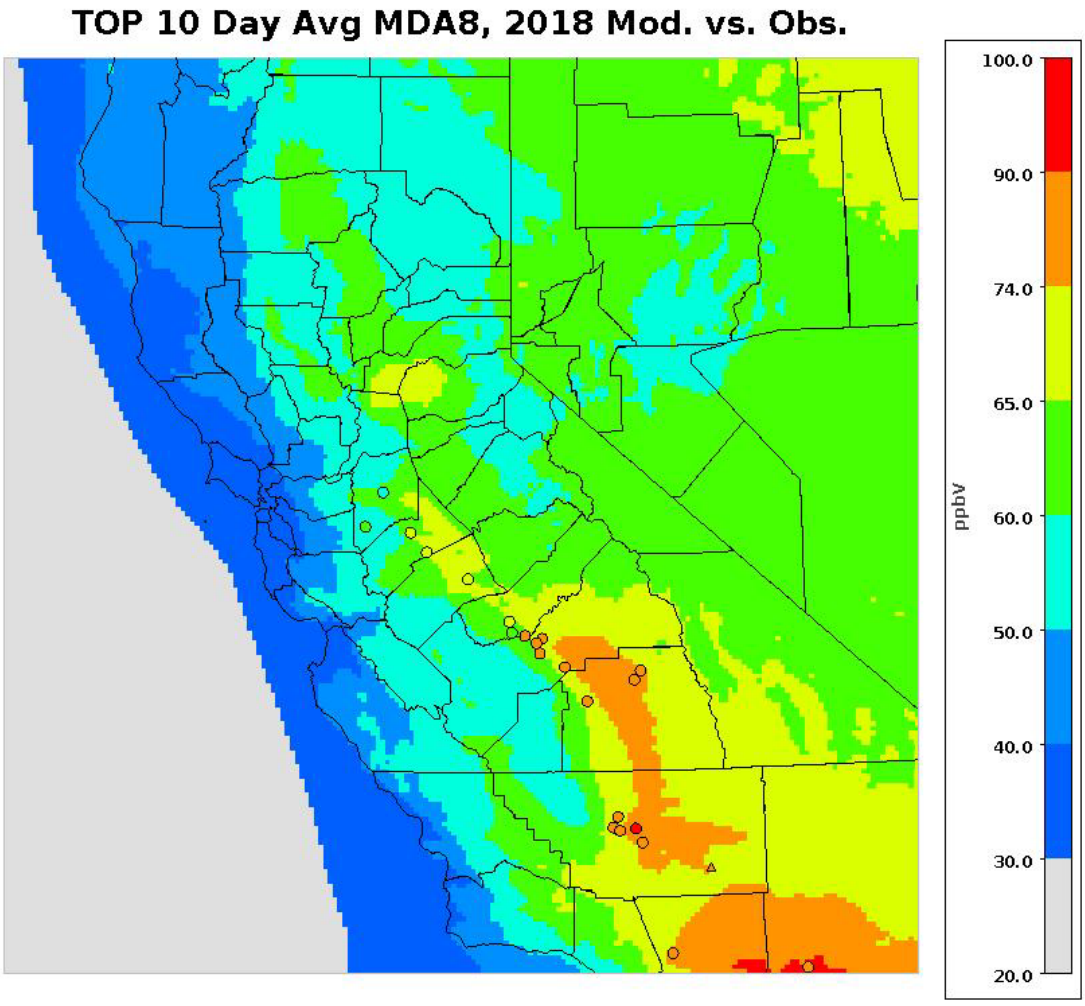

Spatial distributions of modeled and observed average maximum daily average 8-hour ozone for the top 10 O_3 days at the Mojave-923 Poole Street site are displayed in Figure 17. The observation data are from the monitoring sites located in SJV, EKNA and SoCAB that are within the modeling domain. The model is able to capture the observed spatial gradient of ozone in the modeling domain with good agreement between model and observation at the Mojave-923 Poole Street site. Additional analysis including time series of the hourly, maximum daily average 1-hr and maximum daily average 8-hour ozone data at Mojave-923 Poole Street site as well as the time series of NO_2 at a nearby SJV site (Shafter) and a nearby SoCAB site (Santa Clarita) can be found in the supplemental materials.

D. Air Quality Model Diagnostic Evaluation

In addition to the statistical evaluation presented above, since the modeling is utilized in a relative sense, it is also useful to consider whether the model is able to reproduce observable relationships between changes in emissions and ozone. One approach to this would be to conduct a retrospective analysis where additional years are modeled (e.g., 2000 or 2005) and then investigate the ability of the modeling system to reproduce the observed changes in ozone over time. Since this approach is extremely time consuming and resource intensive, it is generally not feasible to perform such an analysis under the constraints of a typical SIP modeling application. An alternative approach for investigating the ozone response to changes in emissions is through the so called "weekend effect".

The "weekend effect" is a well-known phenomenon in some major urbanized areas where emissions of NO_x are substantially lower on weekends than on weekdays, but measured levels of ozone are higher on weekends than on weekdays. This is due to the complex and non-linear relationship between NO_x and ROG precursors and ozone (e.g., Sillman, 1999).

In general terms, under ambient conditions of high-NO_x and low-ROG (NO_x-disbenefit region in Figure 18 ozone formation tends to exhibit a disbenefit to reductions in NO_x emissions (i.e., ozone increases with decreases in NO_x) and a benefit to reductions in ROG emissions (i.e., ozone decreases with decreases in ROG). In contrast, under ambient conditions of low-NO_x and high-ROG (NO_x-limited region in Figure 18), ozone formation shows a benefit to reductions in NO_x emissions, while changes in ROG emissions result in only minor decreases in ozone. These two distinct "ozone chemical regimes" are illustrated in Figure 18 along with a transitional regime that can exhibit characteristics of both the NO_x-disbenefit and NOx-limited regimes. Note that Figure 18 is shown for illustrative purposes only and does not represent the actual ozone sensitivity within the EKNA for a given combination of NO_x and ROG (VOC) emissions.

In this context, the prevalence of a weekend effect in a region suggests that the region is in a NO_x-disbenefit regime. A lack of a weekend effect (i.e., no pronounced high O_3 occurrences during weekends) would suggest that the region is in a transition regime and moving between exhibiting a NO_x-disbenefit and being NO_x-limited. A reversed weekend effect (i.e., lower O_3 during weekends) would suggest that the region is NO_x-limited.

Figure 18. Illustration of a typical ozone isopleth plot, where each line represents ozone mixing ratio, in 10 ppb increments, as a function of initial NOx and VOC (or ROG) mixing ratio (adapted from Seinfeld and Pandis, 1998, Figure 5.15). General chemical regimes for ozone formation are shown as NOx-disbenefit (red circle), transitional (blue circle), and NOx-limited (green circle).

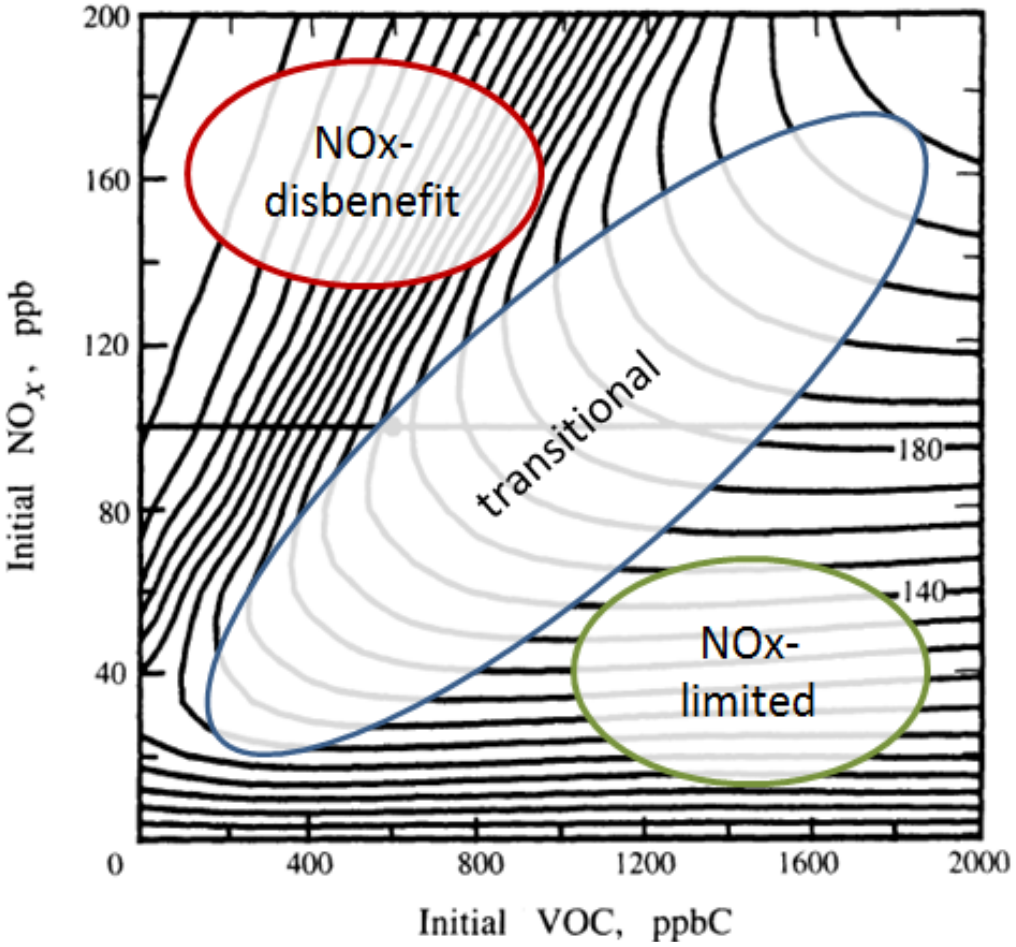

Figure 19. Site-specific average weekday and weekend maximum daily average 8-hour ozone for each year from 2000 to 2020 in the EKNA. The colored circle markers denote observed values while the black square, triangle add diamond markers denote the simulated baseline 2018, future years 2026 and 2032 values. Points falling below the 1:1 dashed line represent a NO_x-disbenefit regime, those on the 1:1 dashed line represent a transitional regime, and those above the 1:1 dashed line represent a NO_x-limited regime.

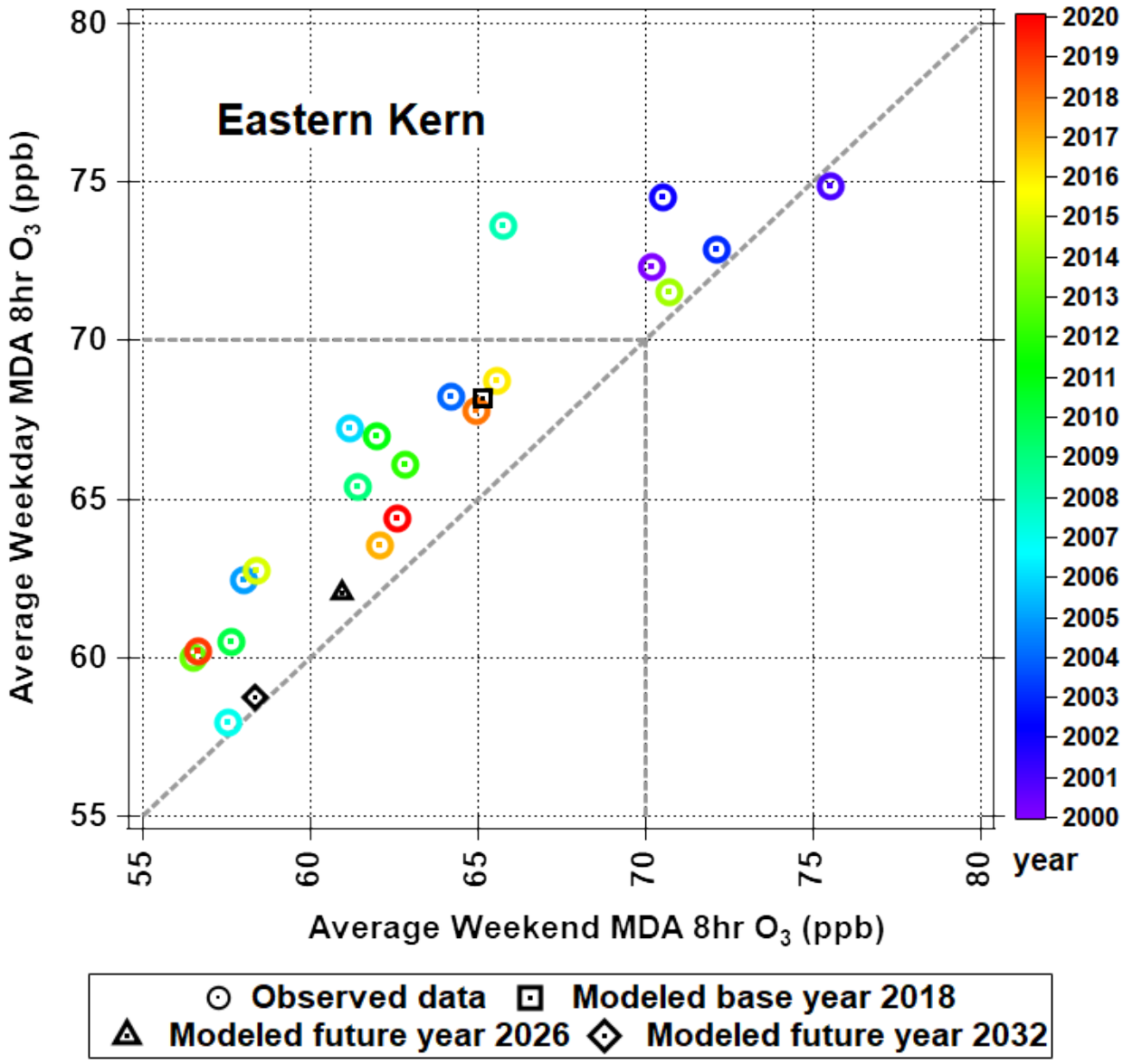

Investigating the "weekend effect" and how it has changed over time is a useful real-world metric for evaluating the ozone chemistry regime in the EKNA and how well it is represented in the modeling. The trend in day-of-week dependence in the EKNA was analyzed using the ozone observations between 2000 and 2020 and the average site-specific weekday (Wednesday and Thursday) and weekend (Sunday) observed summertime (June through September) maximum daily average 8-hour ozone values by year (2000 to 2020) are compared (Figure 19). Different definitions of weekday and weekend days were also investigated and did not show appreciable differences from the Wednesday/Thursday and Sunday definitions.

A key observation in Figure 19 is that the summertime average weekday and weekend ozone levels have steadily declined between 2000 and 2020. Along with the declining ozone, it can be seen that the EKNA has been in a NO_x limited regime for the past two decades as seen from the greater weekday ozone when compared to the weekend ozone. This region is in close proximity

to biogenic ROG emissions sources and farther away from the anthropogenic NO_x sources, such that low NO_x and high ROG reactivity conditions are prevalent, which is consistent with the region being in a NO_x-limited regime. The occasional shift in weekday/weekend ozone levels closer to the 1:1 dashed line (and in some years crossing over the line) is likely due to interannual variability in meteorological conditions and its impact on the regional transport patterns and local biogenic ROG emissions.

The simulated baseline 2018 weekday/weekend values (black square marker in Figure 19) from the attainment demonstration modeling show greater weekday ozone compared to weekend ozone in the EKNA. These predicted values are consistent with observed findings in 2018 that show a prevalence of NO_x-limited conditions in the EKNA. The predicted future 2026 and 2032 values, denoted by black triangle and diamond markers respectively in Figure 19, clearly show that weekday and weekend ozone decline significantly (all values are below 65 ppb) suggesting that NO_x controls will be more effective than corresponding ROG controls in lowering the ozone levels in the EKNA.

E. Future Design Values in 2026 and 2032

The RRFs and the 2026 and 2032 future ozone design values for the Mojave site of the EKNA were calculated using the procedures outlined in the Methodology section of this document and are summarized in Table 14 and Table 15. The projected ozone design value in 2026 is 74 ppb and in 2032 is 69 ppb at the site. Therefore, the attainment demonstration modeling predicts that the EKNA will attain the 2008 75 ppb 8-hour ozone standard by 2026 and the 2015 70 ppb 8-hour ozone standard by 2032 with the commitments outlined in the SIP.

Table 14. Summary of key parameters related to the future year 2026 ozone design value (DV) calculation.

Site	RRF	2018 Average DV (ppb)	2026 DV (ppb)	2026 Truncated DV (ppb)
Mojave-923PooleSt	0.8979	82.7	74.3	74

Table 15. Summary of key parameters related to the future year 2032 ozone design value (DV) calculation.

Site	RRF	2018 Average DV (ppb)	2032 DV (ppb)	2032 Truncated DV (ppb)
Mojave-923PooleSt	0.8400	82.7	69.5	69

F. NOx/VOC Sensitivity Analysis for Reasonable Further Progress (RFP)

For the Clean Air Act 182(c)(2)(B) Reasonable Further Progress (RFP) requirement for areas classified as Serious nonattainment and above, U.S. EPA guidance allows for NOx substitution to demonstrate the annual 3 percent reduction of ozone precursors if it can be demonstrated that substitution of NOx emission reductions (for ROG reductions) yield equivalent decreases in ozone. Additional U.S. EPA guidance states that certain conditions are needed to use NOx substitution in an RFP demonstration (U.S.EPA 1993). First, an equivalency demonstration must show that cumulative RFP emission reductions are consistent with the NOx and ROG emission reductions determined in the ozone attainment demonstration. Second, the reductions in NOx and ROG emissions should be consistent with the continuous RFP emission reduction requirement.

For the equivalency demonstration, ROG and NOx emissions within the nonattainment area boundary were reduced by 45% (3% for each of the 15 years between the designation year of 2017 and attainment year of 2032) independently from the baseline modeling year of 2018. These sensitivity simulations were used to develop RRFs and design values following the same methodology utilized in the attainment demonstration, where the sensitivity simulation was treated analogous to the future year. Table 16 summarizes the design values calculated for the 45% NOx and ROG sensitivity simulations. At the Mojave site, the ratio of the change in ozone design value to the NOx emissions change ($\Delta O_3/\Delta NOx$) are greater than that of the ROG emissions change ($\Delta O_3/\Delta ROG$). Since the ozone improvement from NOx reductions is greater than that for ROG reductions, the use of NOx substitution will result in improved ozone air quality.

Table 16. Summary of the ozone improvement from the 45% emissions reductions at the monitoring site in the EKNA.

Site	2018 Average DV (ppb)	DV After 45% NOx Reductions (ppb)	$\Delta O_3/\Delta NOx$ (ppb/tpd)	DV After 45% ROG Reductions (ppb)	$\Delta O_3/\Delta ROG$ (ppb/tpd)
Mojave-923PooleSt	82.7	82.2	0.0426	82.7	0.0000

G. Unmonitored Area Analysis

The unmonitored area analysis is used to ensure that there are no regions outside of the existing monitoring network that would exceed the NAAQS if a monitor was present (U.S. EPA, 2018). U.S. EPA recommends combining spatially interpolated design value fields with modeled ozone gradients and grid-specific RRFs in order to generate gridded future year gradient adjusted design values.

This analysis can be done using SMAT-CE (Software for the Modeled Attainment Test – Community Edition, https://www.epa.gov/scram/photochemical-modeling-tools). However, this software is not open source and comes as a precompiled software package. To maintain transparency and flexibility in the analysis, in-house R codes developed at ARB, were utilized in this analysis.

The unmonitored area analysis was conducted using the 8-hr O_3 weighted DVs from all the available sites that fall within the 4 km inner modeling domain along with the reference year 2018 and future years (2026 and 2032) 4 km CMAQ model output. The steps followed in the unmonitored area analysis are as follows:

Step 1: At each grid cell, the top 10 modeled maximum daily average 8-hour ozone mixing ratios from the reference year simulation were averaged, and a gradient in this top 10 day average between each grid cell and grid cells which contain a monitor was calculated.

Step 2: A single set of spatially interpolated 8-hour ozone DV fields was generated based on the observed 5-year weighted base year 8-hour ozone DVs from the available monitors. The interpolation is done using normalized inverse distance squared weightings from each monitor within the Voronoi regions that boarder that of the grid cell (calculated with the R tripack library), and adjusted based on the gradients between the grid cell and the corresponding monitor from Step 1.

Step 3: At each grid cell, the RRFs are calculated based on the reference- and future-year modeling following the same approach outlined in in the Methodology section of this document, except that the +/- 20% limitation on the simulated and observed maximum daily average 8-hour ozone was not applied because observed data do not exist for grid cells in unmonitored areas.

Step 4: The future year gridded 8-hour ozone DVs were calculated by multiplying the gradient-adjusted interpolated 8-hour ozone DVs from Step 2 with the gridded RRFs from Step 3

Step 5: The future-year gridded 8-hour ozone DVs (from Step 4) were examined to determine if there are any peak values higher than those at the monitors, which could potentially cause violations of the applicable 8-hour ozone NAAQS.

Under the Voronoi diagram method, each monitoring site was assigned to a Voronoi region based on location and the distance to each grid cell (Sen 2016), and the interpolations were done between each grid cell and all the monitors in surrounding Voronoi regions. Voronoi diagram with inverse distance weighting method has been used in various 2-D data analysis areas, including air quality measurements interpolations (Atsuyuki, et al., 2009; Deligiorgi and Philippopoulos 2011).

The spatial distribution of gridded DVs in 2026 (left panel) and 2032 (right panel) for the EKNA unmonitored area analysis (described above) are shown in Figure 20. The black colored star markers denote the monitoring sites, which had valid reference year 2018 DVs and were used in the analysis. The unmonitored area analysis for future year 2026 in the EKNA shows an area within the region located to the center of the western boundary, which has 2026 DVs greater than 75 ppb. The 2032 unmonitored area analysis shows some isolated spots located close to the southern boundary with future DVs above 70 ppb.

Wildfires have significantly impacted the SJVAB and EKNA ozone levels over the past years (Weight of Evidence of this SIP document and SJV 2022). Fire impacted days from 2016 – 2019 that influenced the ozone DVs within the SJVAB and EKNA are listed in Table S 1. Figure 21 shows the spatial distribution of interpolated future year ozone DVs within EKNA when fire impacted days were excluded from the base year DV calculations for both the SJVAB and EKNA monitoring sites. Compared to the results shown in Figure 20, there is a clear decrease in ozone DVs across the entire region for both 2026 and 2032. The non-attainment area in the center along the western boundary for 2026 is much smaller after fire days are excluded. For year 2032, the entire EKNA will attain the 70 ppb standard with fire days excluded.

The small non-attainment area in 2026 is in close proximity and lies directly downwind of the SJVAB. Based on the phenomenological evaluation of the wind fields shown in the bottom panel of Figure 13, there were prevailing westerly winds at mid-day during the top 10 ozone days, indicating significant contributions from regional transport of emissions in the SJVAB/Bakersfield region to the ozone levels in EKNA. In contrast, due to the mountains (see terrain plots in Figure 22) that separate EKNA from SJVAB in the west, the unmonitored region exhibiting elevated ozone levels in 2026 is generally isolated from air pollutants emitted in other regions of the EKNA.

From 2026 to 2032, the unmonitored area that exceeded the 75 ppb standard in 2026 is predicted to experience a decrease in ozone of over 5 ppb, bringing the region into attainment of the 70 ppb standard. Over that same time period, emissions of NOx and ROG in the EKNA are predicted to decrease very little from 17.8 tpd and 7.0 tpd to 17.5 tpd and 6.8 tpd, respectively. In contrast, NOx and ROG emissions in the SJVAB are predicted to decrease much more significantly, particularly for NOx, from 126 tpd and 296 tpd in 2026 to 100 tpd and 290 tpd in 2032, respectively. Given the predominant wind patterns and topography, it is clear that the unmonitored region along the western boundary between EKNA and SJVAB is influenced more by emissions from the SJVAB than from EKNA and that as SJVAB emissions are reduced, the unmonitored region will be brought into attainment of both the 75 ppb and 70 ppb ozone standards.

Figure 20. Spatial distribution of the future 2026 DVs (left) and 2032 DVs (right) based on the unmonitored area analysis in the EKNA.

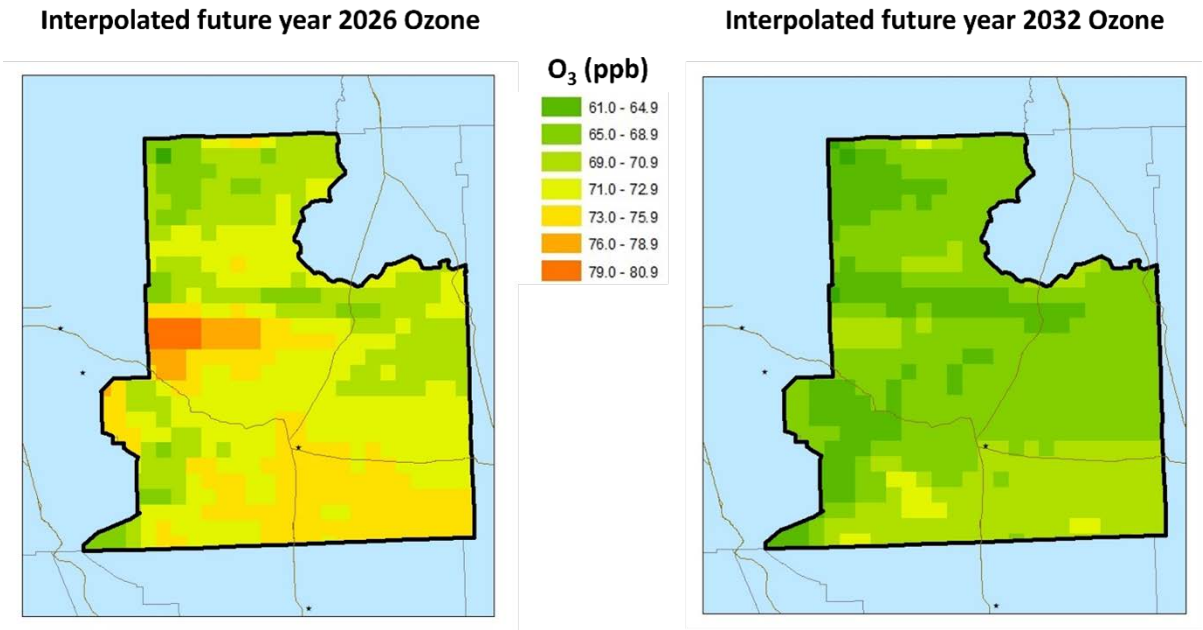

Figure 21. Spatial distribution of the future 2026 DVs (left) and 2032 DVs (right) based on the unmonitored area analysis in the EKNA, with fire days excluded in DVs calculation for EKNA and SJV sites.

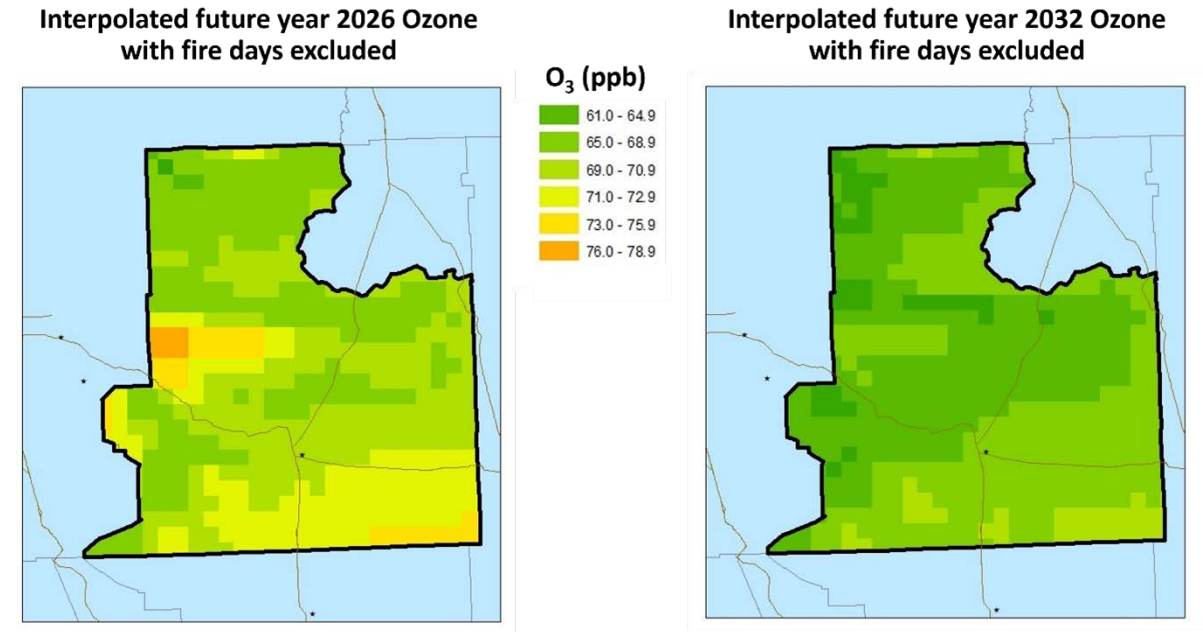

Figure 22. Terrain plots of EKNA and surrounding regions, with mark of grids that have interpolated 2026 Ozone concentration above standard (75 ppb) based on the unmonitored area analysis in the EKNA. Blue bordered grids in the figures represent the area that have interpolated 2026 ozone concentration above standard (75 ppb), with fire days included (left) and excluded (right) in DVs calculation for EKNA and SJV sites.

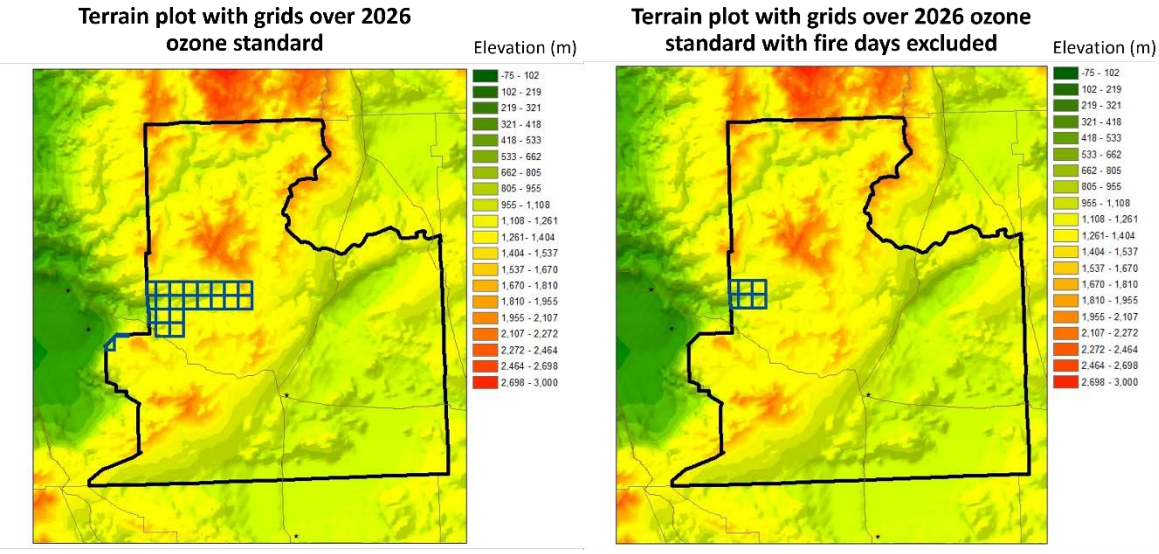

References

Angevine, W. M., L. Eddington, K. Durkee, C. Fairall, L. Bianco, and J. Brioude. 2012. "Meteorological model evaluation for CalNex 2010." *Monthly Weather Review* (140): 3885-3906.

Atsuyuki, O., B. Boots, K. Sugihara, and S. N. Chiu. 2009. *Spatial tessellations: concepts and applications of Voronoi diagrams.* Second. John Wiley & Sons.

Baker, K. R., C. Misenis, M. D. Obland, R. A. Ferrare, A. J. Scarino, and J. T. Kelly. 2013. "Evaluation of surface and upper air fine scale WRF meteorological modeling of the May and June 2010 CalNex period in California." *Atmospheric Environment* (80): 299-309.

Bao, J.W., S.A. Michelson, P.O.G. Persson, I.V. Djalalova, and J.M. Wilczak. 2008. "Observed and WRF-simulated low-level winds in a high-ozone episode during the Central California ozone study." *Journal of Applied Meteorology and Climatology* 47: 2372-2394.

Beaver, S., and A. Palazoglu. 2009. "Influence of synoptic and mesoscale meteorology on ozone pollution potential for San Joaquin Valley of California." *Atmospheric Environment* 43 (10).

Blanchard, C.L., S. Tanenbaum, E.M. Fujita, D. Campbell, and J. Wilkinson. 2008. *Understanding Relationships between Changes in Ambient Ozone and Precursor Concentrations and Changes in VOC and NOx Emissions from 1990 to 2004 in Central California.* Report prepared for the California Air Resources Board, Envair, DRI and Alpine Geophysics.

Buchholz, R. R., Emmons, L. K., Tilmes, S., & The CESM2 Development Team. 2019. "CESM2.1/CAM-chem Instantaneous Output for Boundary Conditions." UCAR/NCAR - Atmospheric Chemistry Observations and Modeling Laboratory. https://doi.org/10.5065/NMP7-EP60.

Cai, C., J. C. Avise, A. Kaduwela, J. DaMassa, C. Warneke, J. B. Gilman, W. Kuster, et al. 2019. "Simulating the Weekly Cycle of NOx-VOC-HOx-O3Photochemical System in the South Coast ofCalifornia During CalNex-2010 Campaign." *Journal of Geophysical Research: Atmospheres* 3532–3555.

Cai, C., S. Kulkarni, Z. Zhao, A. Kaduwela, J. C. Avise, and J. A. DaMassa. 2016. "Simulating Reactive Nitrogen, Carbon Monoxide, and Ozone in California During ARCTAS-CARB 2008 with High Wildfire Activity." *Atmospheric Environment* 28-44.

CARB. 1990. *Assessment and Mitigation of the Impacts of Transported Pollutants on Ozone Concentrations within California, Staff Report prepared by the Technical Support Division and the Office of Air Quality Planning and Liaison of the California Air Resources Board.* available at https://www.arb.ca.gov/aqd/transport/assessments/1990.pdf.

CARB. 2020. *2017 Baseline Inventory and Vehicle Miles Traveled Offset Demonstration for the 2015 70 ppb 8-hour Ozone Standard available at*

https://ww2.arb.ca.gov/resources/documents/2017-baseline-inventory-and-vehicle-miles-traveled-offset-demonstration-2015-70. Accessed Jan 2022.

CARB. 2018. "2018 Western Nevada County Planning Area Ozone Attainment Plan available at https://ww3.arb.ca.gov/planning/sip/planarea/wnc/carb_staff_report.pdf." Staff Report. Accessed Jan 2022.

Carter, W.P.L. 2010b. "Development of a condensed SAPRC-07 chemical mechanism." *Atmospheric Environment* 5336-5345.

Carter, W.P.L. 2010a. "Development of the SAPRC-07 chemical mechanism." *Atmospheric Environment* 5324-5335.

Chen, J., D. Yin, Z. Zhao, A. P. Kaduwela, J. C. Avise, J. A. DaMassa, A. Beyersdorf, and S. Burton et al. 2020. "Modeling air quality in the San Joaquin Valley of California during the 2013 DISCOVER-AQ field campaign." *Atmospheric Environment* (5): 100067.

Deligiorgi, D., and K. Philippopoulos. 2011. "Spatial Interpolation Methodologies in Urban Air Pollution Modeling: Application for the Greater Area of Metropolitan Athens, Greece." In *Advanced Air Pollution*. doi:10.5772/17734.

EasternKern. 2017. "2017 Ozone Attainment Plan, available at: http://www.kernair.org/Documents/Announcements/Attainment/2017%20Ozone%20Plan_EKAPCD_Adopted_7-27-17.pdf."

EKAPCD. 2003. "East Kern County Ozone Attainment Demonstration, Maintenance Plan, and Redesignation Request." available at https://www.arb.ca.gov/planning/sip/planarea/easternkern/2003kernplan.pdf.

Emery, C., Liu, Z., Russell, A. M., Odman, T., Yarwood, G., Kumar, N. 2017. "Recommendations on statistics and benchmarks to assess photochemical model performance." *Journal of the Air & Waste Management Association* 582-598.

Emmons, L. K., R. H. Schwantes, J. J. Orlando, G. Tyndall, D. Kinnison, and J.-F. Lamarque et al. 2020. "The Chemistry Mechanism in the Community Earth System Model version 2 (CESM2)." *Journal of Advances in Modeling Earth Systems.* https://doi.org/10.1029/2019MS001882.

EPA, U.S. 2017. "Ozone Designations - 2015 Standards accessible at https://www.epa.gov/sites/default/files/2018-05/documents/ca_tsd_combined_final_0.pdf." Accessed Jan 2022. https://www.epa.gov/sites/default/files/2018-05/documents/ca_tsd_combined_final_0.pdf.

Fast, J. D., W. I. Gustafson Jr, L. K. Berg, W. J. Shaw, M. Pekour, and M. Shrivastava et al. 2012. "Transport and mixing patterns over Central California during the carbonaceous aerosol and radiative effects study (CARES)." *Atmospheric Chemistry and Physics* (12): 1759-1783.

Fosberg, M.A., and M.J. Schroeder. 1966. "Marine air penetration in Central California." *Journal of Applied Meteorology* (5): 573-589.

Fujita, E. M., R. E. Keislar, D. L. Freeman, J. Watson, A. J. Ranzieri, S. Tanrikulu, and K. Magliano. 1999. *Field study plan for the Central California Ozone Study.*

He, H., X-Z. Liang, and D. J. Wuebbles. 2018. "Effects of emissions change, climate change and long-range transport on regional modeling of future U.S. particulate matter pollution and speciation." *Atmospheric Environment*, 166-176. doi:https://doi.org/10.1016/j.atmosenv.2018.02.020.

Heuss, J. M., D. F. Kahlbaum, and G. T. Wolff. 2003. "Weekday/Weekend Ozone Differences: What Can We Learn from Them?" *Journal of the Air & Waste Management Association* 53 (7): 772-788.

Hu, J., C. J. Howard, F. Mitloehner, P. G. Green, and M. J. Kleeman. 2012. "Mobile Source and Livestock Feed Contributions to Regional Ozone Formation in Central California." *Environmental Science and Technology* (46): 2781-2789.

Imperial. 2017. " Imperial County 2017 State Implementation Plan for the 2008 8-Hour Ozone Standard, available at: https://ww3.arb.ca.gov/planning/sip/planarea/imperial/2017o3sip_final.pdf ."

Imperial. 2018. " Imperial County 2018 Annual Particulate Matter Less than 2.5 Microns in Diameter State Implementation Plan, available at: https://ww3.arb.ca.gov/planning/sip/planarea/imperial/final_2018_ic_pm25_sip.pdf ."

Jin, L., N. J. Brown, R. A. Harley, J-W. Bao, S. A. Michelson, and J. M. Wilczak. 2010. "Seasonal versus episodic performance evaluation for an Eulerian photochemical air quality model." *Journal of Geophysical Research: Atmospheres* 115, D09302.

Jin, L., S. Tonse, D. S. Cohan, X Mao, R. A. Harley, and N. J. Brown. 2008. "Sensitivity analysis of ozone formation and transport for a central California air pollution episode." *Environmental Science and Technology* 3683-3689.

Kelly, J. T., K. R. Baker, J. B. Nowak, J. G. Murphy, Z. M. Milos, T. C. VandenBoer, R. A. Ellis, et al. 2014. "Fine-scale simulation of ammonium and nitrate over the South Coast Air Basin and San Joaquin Valley of California during CalNex-2010." *Journal of Geophysical Research* (119): 3600-3614. doi:doi:10.1002/2013JD021290.

Kelly, J.T., J. Avise, C. Cai, and A. Kaduwela. 2010. "Simulating particle size distributions over California and impact on lung deposition fraction." *Aerosol Science and Technology* 148-162.

Kelly, J.T., K.R Baker, J.B. Nowak, and J.G Murphy et al. 2014. "Fine-scale simulation of ammonium and nitrate over the South Coast Air Basin and San Joaquin Valley of California during CalNex-2010." *Journal of Geophysical Research: Atmosphere* 3600–3614.

Kulkarni, S., A. P. Kaduwela, J. C. Avise, J. A. DaMassa, and D. Chau. 2014. "An extended approach to calculate the ozone relative response factors used in the attainment demonstration for the National Ambient Air Quality Standards." *Journal of the Air and Waste Management Association* 1204-1213.

Lamarque, J.-F., L. K. Emmons, P. G. Hess, D. E. Kinnison, S. Tilmes, F. Vitt, C. L. Heald, et al. 2012. "CAM-chem: description and evaluation of interactive atmospheric chemistry in the Community Earth System Model." *Geoscientific Model Development* 369-411.

Lehrman, D. 2001. *Characterization of the 2000 Measurement Period.* Interim Report prepared for California Air Resources Board, Technical and Business Systems, Inc.,.

Lehrman, D., D. Bush, B. Knuth, D. Fairley, and C. Blanchard. 2004. *Characterization of the CCOS 2000 measurement period.* Final Report prepared for California Air Resources Board, Technical and Business Systems, Inc.

Lin, M., A. M. Fiore, O. R. Cooper, L. W. Horowitz, A. O. Langford, H. Levy II, B. J. Johnson, V. Naik, and S. J. Oltmans. 2012. "Springtime high surface ozone events over the western United States: Quantifying the role of stratospheric." *Journal of Geophysical Research* D00V22, doi:10.1029/2012JD018151.

Livingstone, P.L., K. Magliano, K. Gurer, P.D. Allen, K.M. Zhang, Q. Ying, and , B.S. Jackson et al. 2009. "Simulating PM concentration during a winter episode in a subtropical valley: Sensitivity simulations and evaluation methods." *Atmospheric Environment* 5971-5977.

Pun, B. K., J. F. Loius, and C. Seigneur. 2008. *A conceptual model of ozone formation in the San Joaquin Valley.* CP049-1-98, Atmospheric and Environmental Research Inc., San Ramon, CA.

Pun, B.K., R.T.F. Balmori, and C. Seigneur. 2009. "Modeling wintertime particulate matter formation in central California." *Atmospheric Environment* 402-409.

Pusede, S. E., and R. C. Cohen. 2012. "On the observed response of ozone to NOx and VOC reactivity reductions in San Joaquin Valley California 1995–present." *Atmospheric Chemistry and Physics* 8323-8339.

Pusede, S. E., D. R. Gentner, P. J. Wooldridge, E. C. Browne, A. W. Rollins, K. E. Min, A. R. Russell, et al. 2014. "On the temperature dependence of organic reactivity, nitrogen oxides, ozone production, and the impact of emission controls in San Joaquin Valley, California." *Atmospheric Chemistry and Physics* 3373-3395.

Sacramento. 2017. "Sacramento Regional 2008 NAAQS 8-Hour Ozone Attainment And Reasonalbe Further Progress Plan, available at http://www.airquality.org/ProgramCoordination/Documents/Sac%20Regional%202008%20NAAQS%20Attainment%20and%20RFP%20Plan.pdf."

Seinfeld, J. H., and S. N. Pandis. 1998. *Atmospheric Chemistry and Physics: From Air Pollution to Climate Change.* Edited by 1. New York: J. Wiley.

Sen, Zekai. 2016. "2.8.1 Delaney, Varoni, and Thiessen Polygons." In *Spatial Modeling Principles in Earth Sciences*, 57. Springer.

Shahrokhishahraki, N., P. J. Rayner, J. D. Silver, S. Thomas, and R. Schofield. 2022. "High-resolution modeling of gaseous air pollutants over Tehran and validation with surface and satellite data." *Atmospheric Environment.* doi:https://doi.org/10.1016/j.atmosenv.2021.118881.

Shearer, S. M., Harley, R. A., Jin, L., Brown, N. J. 2012. "Comparison of SAPRC99 and SAPRC07 mechanisms in photochemical modeling for central California." *Atmospheric Environment* 205-216.

Sillman, S. 1999. "The relation between ozone, NOx and hydrocarbons in urban and polluted rural environments." *Atmospheric Environment* 33 (12): 1821-1845.

Simon, H., K. R. Baker, and S. Phillips. 2012. "Compilation and interpretation of photochemical model performance statistics published between 2006 and 2012." *Atmospheric Environment* (61): 124-139.

SJV. 2018. " 2018 PM2.5 Plan for the San Joaquin Valley, available at: http://valleyair.org/pmplans/ ."

SJV. 2008. "2008 PM2.5 Plan, available at: http://www.valleyair.org/Air_Quality_Plans/AQ_Proposed_PM25_2008.htm."

SJV. 2012. "2012 PM2.5 Plan, available at: http://www.valleyair.org/Air_Quality_Plans/PM25Plans2012.htm ."

SJV. 2013. "2013 Plan for the Revoked 1-Hour Ozone Standard, available at: http://valleyair.org/Air_Quality_Plans/Ozone-OneHourPlan-2013.htm ."

SJV. 2016a. "2016 Moderate Area Plan for the 2012 PM2.5 Standard, available at: http://www.valleyair.org/Air_Quality_Plans/docs/PM25-2016/2016-Plan.pdf ."

SJV. 2016b. "2016 Plan for the 2008 8-Hour Ozone Standard, available at: http://valleyair.org/Air_Quality_Plans/Ozone-Plan-2016.htm ."

Skamarock, W. C., J. B. Klemp, J. Dudhia, D. O. Gill, D. M. Barker, M. G. Duda, X.-Y. Huang, W. Wang, and J. G. Powers. 2008. ""Description ofthe Advanced Research WRF version 4,Rep. NCAR/TN-475++STR,Natl. Cent. for Atmos. Res., "." Boulder, Colo.

SouthCoast. 2012. "Final 2012 Air Quality Management Plan, available at: http://www.aqmd.gov/home/air-quality/clean-air-plans/air-quality-mgt-plan/final-2012-air-quality-management-plan ."

SouthCoast. 2016. "Final 2016 Air Quality Management Plan, available at: http://www.aqmd.gov/docs/default-source/clean-air-plans/air-quality-management-plans/2016-air-quality-management-plan/final-2016-aqmp/cover-and-opening.pdf?sfvrsn=6."

Tonse, S. R., N. J. Brown, R. A. Harley, and L. Jin. 2008. "A process-analysis based study of the ozone weekend effect." *Atmospheric Environment* 7728-7736.

U.S. EPA. 2018. *Modeling Guidance for Demonstrating Attainment of Air Quality Goals for Ozone, PM2.5, and Regional Haze.* 11 29. https://www.epa.gov/scram/sip-modeling-guidance-documents.

U.S.EPA. 1993. "NOx Substitution Guidance, available at https://www3.epa.gov/ttn/naaqs/aqmguide/collection/cp2/19931201_oaqps_nox_substitution_guidance.pdf."

Ventura. 2016. "Final 2016 Ventura County Air Quality Management Plan, available at: http://www.vcapcd.org/pubs/Planning/AQMP/2016/Final/Final-2016-Ventura-County-AQMP.pdf ."

Vijayaraghavan, K., P. Karamchadania, and C. Seigneur. 2006. "Plume-in-grid modeling of summer air pollution in Central California." *Atmospheric Environment* 5097-5109.

Wang, P., P. Wang, K. Chen, J. Du, and H Zhang. 2022. "Ground-level ozone simulation using ensemble WRF/Chem predictions over the Southeast United States." *Chemosphere.* doi:https://doi.org/10.1016/j.chemosphere.2021.132428.

WesternMojave. 2016. "2016 8-Hour Ozone SIP: Western Mojave Desert Nonattainment Area, available at: https://ww3.arb.ca.gov/planning/sip/planarea/mojavesedsip.htm#2016."

WesternNevada. 2018. "Western Nevada County 8-hour Ozone Attainment Plan, available at: https://ww3.arb.ca.gov/planning/sip/planarea/wncsip.htm."

Yan, F., Y. Gao, M. Ma, C. Liu, X. Ji, F. Zhao, X. Yao, and H. Gao. 2021. "Revealing the modulation of boundary conditions and governing processes on ozone formation over northern China in June 2017." *Environmental Pollution* 272. doi:https://doi.org/10.1016/j.envpol.2020.115999.

Yienger, J. J., and H. Levy II. 1995. "Empirical model of global soil-biogenic NOχ emissions." *Journal of Geophysical Research: Atmospheres* 11447-11464.

Zhang, Y., P. Liu, X. Liu, B. Pun, C. Seigneur, M.Z. Jacobson, and W. Wang. 2010. "Fine scale modeling of wintertime aerosol mass, number, and size distributions in Central California." *Journal of Geophysical Research* D15207, doi:10.1029/2009JD012950.

Zhu, S., Horne, J. R., Kinnon, M. M., Samuelsen, G. S., Dabdub, D. 2019. "Comprehensively assessing the drivers of future air quality in California." *Environment International* 386-398.

IV. Supplemental Materials

Supplemental Materials List of Figures

Figure S 1. Time series of average temperature, relative humidity, wind speed, and direction of all sites in April 2018. 58

Figure S 2. Time series of average temperature, relative humidity, wind speed, and direction of all sites in May 2018. 59

Figure S 3. Time series of average temperature, relative humidity, wind speed, and direction of all sites in June 2018. 60

Figure S 4. Time series of average temperature, relative humidity, wind speed, and direction of all sites in July 2018..... 61

Figure S 5. Time series of average temperature, relative humidity, wind speed, and direction of all sites in August 2018. 62

Figure S 6. Time series of average temperature, relative humidity, wind speed, and direction of all sites in September 2018..... 63

Figure S 7. Time series of average temperature, relative humidity, wind speed, and direction, and temperature of all sites in October 2018. 64

Figure S 8. Observed and modeled ozone frequency distribution at the Mojave-923PooleSt site for the ozone season (April – October 2018) 65

Figure S 9. Observed and modeled ozone scatter plots at the Mojave-923PooleSt site for the ozone season (April – October 2018) 66

Figure S 10. Time-series of hourly ozone at Mojave-923PooleSt for the ozone season (April – October 2018) 67

Figure S 11. Time-series of maximum daily 1-hour ozone at the Mojave-923PooleSt site for the ozone season (April – October 2018) 67

Figure S 12. Time-series of maximum daily average 8-hour ozone at the Mojave-923PooleSt site for the ozone season (April – October 2018) 67

Figure S 13. Time-series of hourly NO_2 at the Shafter site in San Joaquin Valley for the ozone season (April-October 2018)..... **Error! Bookmark not defined.**

Figure S 14. Time-series of hourly NO_2 at the Santa Clarita site in South Coast for the ozone season (April-October 2018)..... 69

Figure S 1. Time series of average temperature, relative humidity, wind speed, and direction of all sites in April 2018.

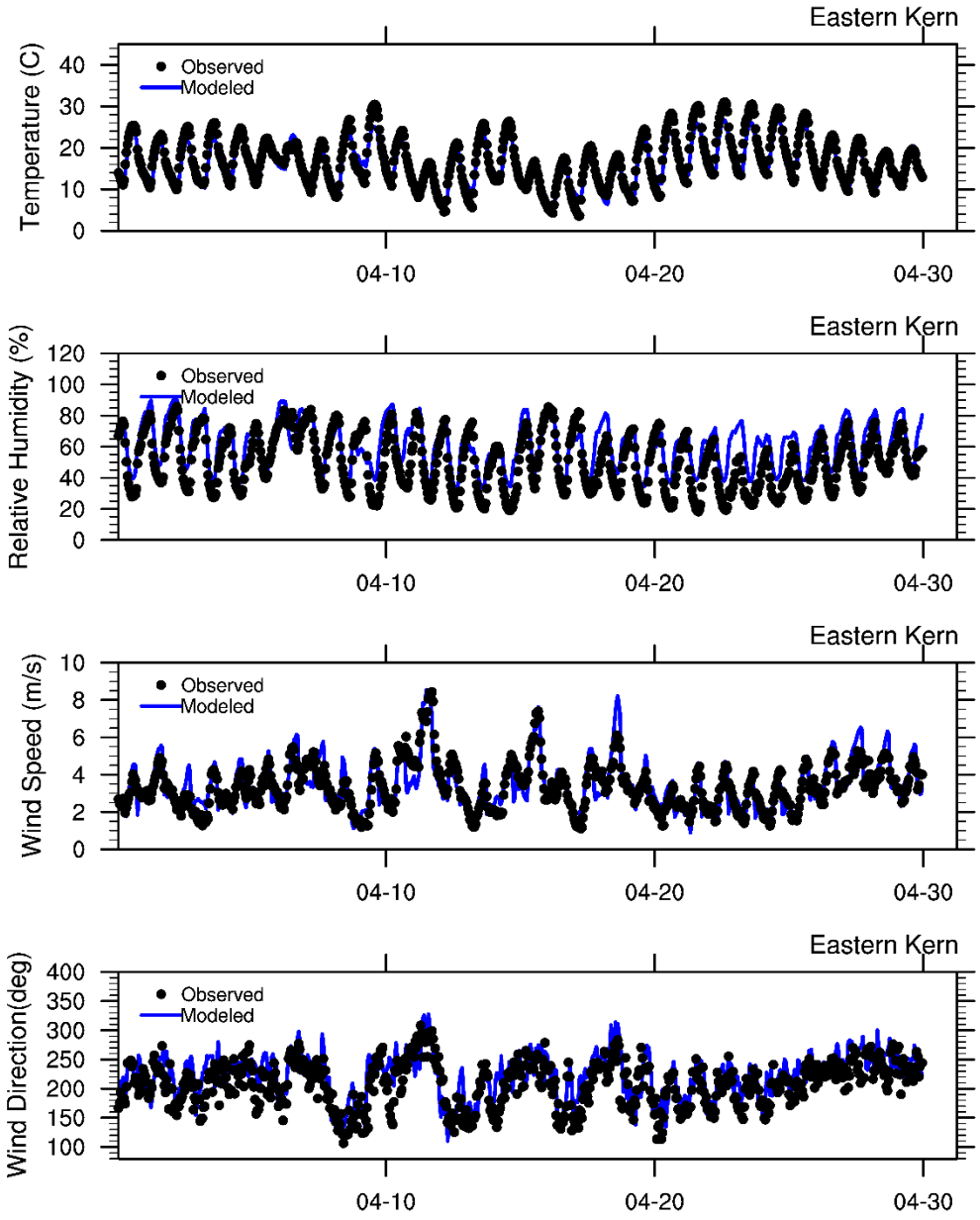

Figure S 2. Time series of average temperature, relative humidity, wind speed, and direction of all sites in May 2018.

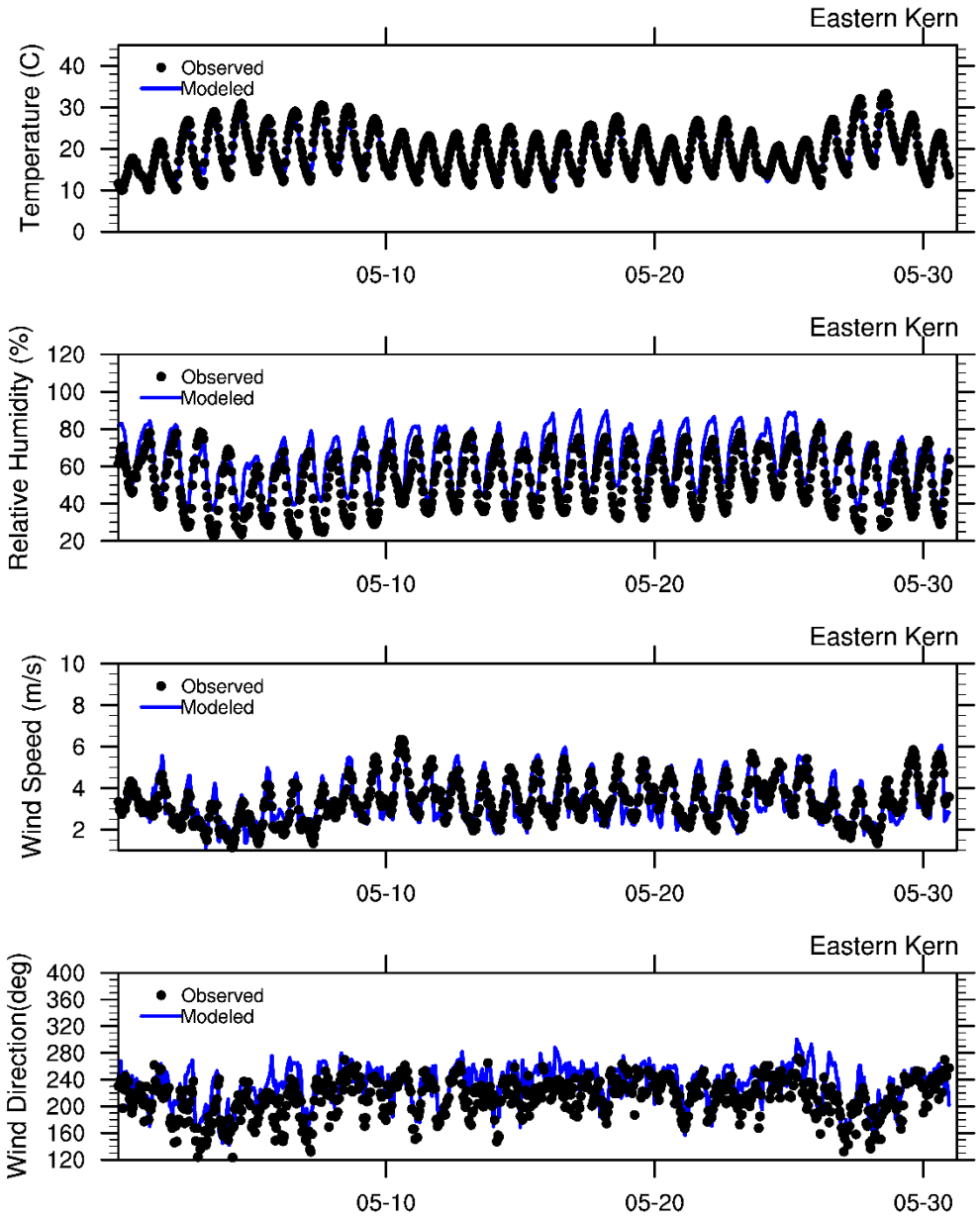

Figure S 3. Time series of average temperature, relative humidity, wind speed, and direction of all sites in June 2018.

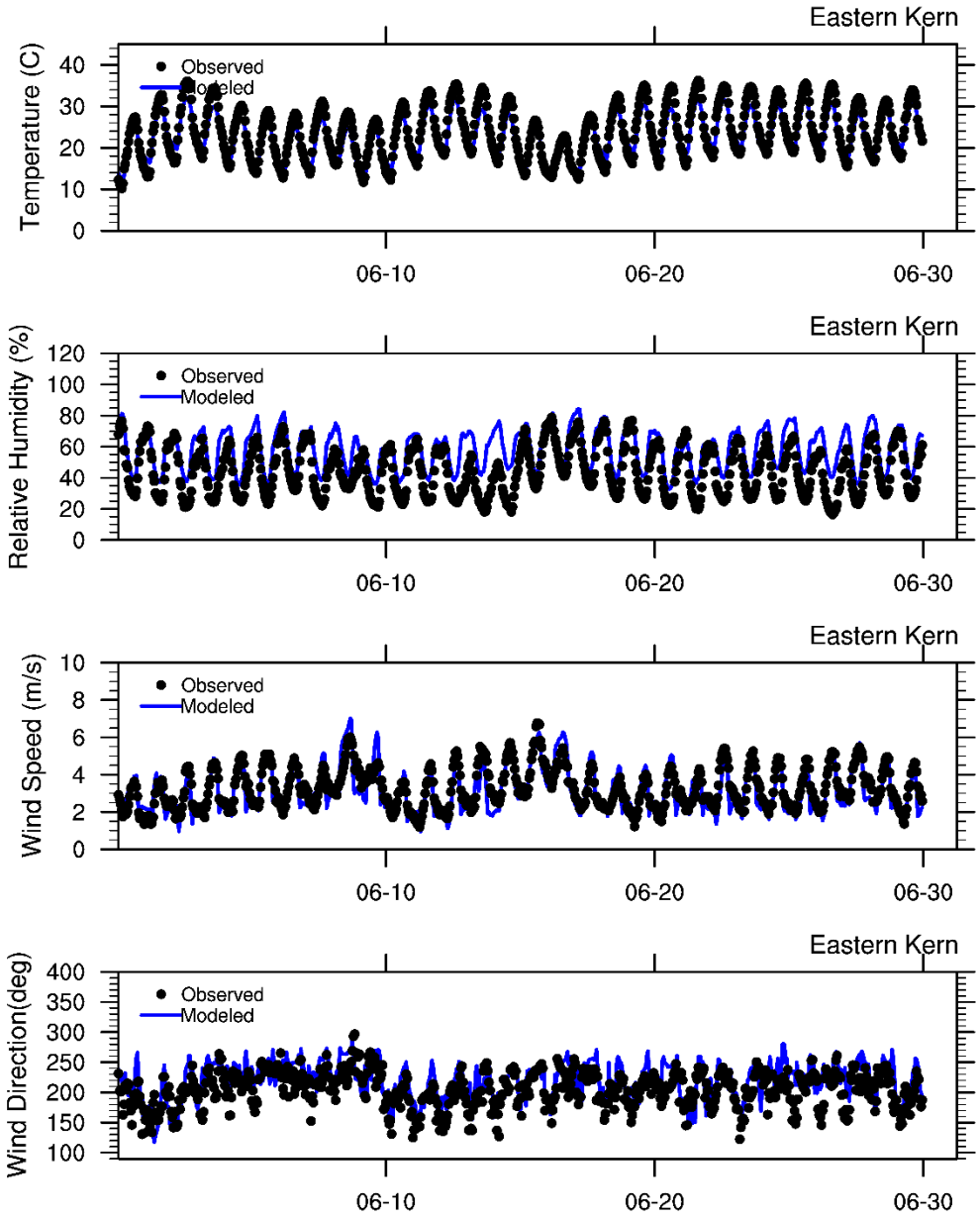

Figure S 4. Time series of average temperature, relative humidity, wind speed, and direction of all sites in July 2018.

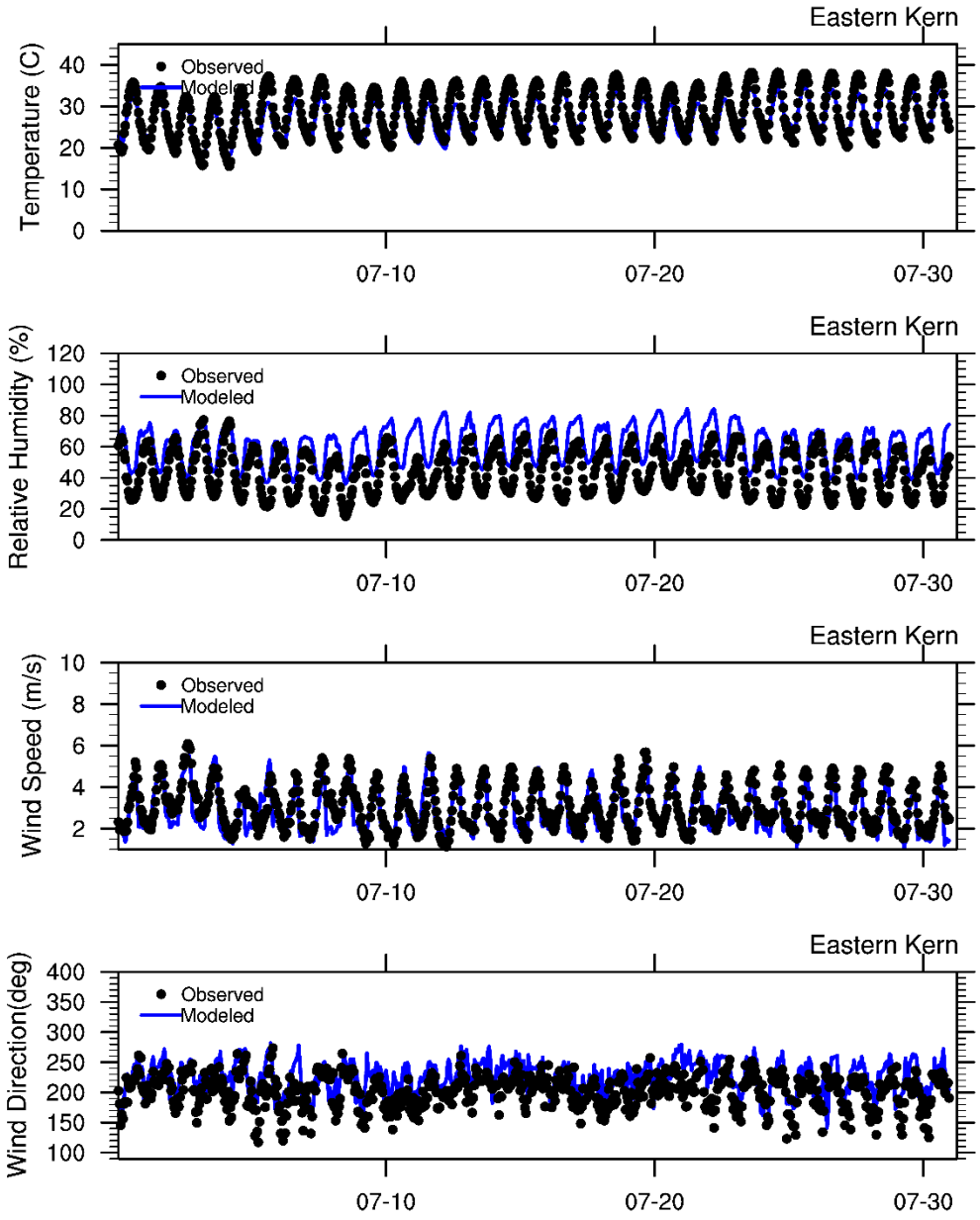

Figure S 5. Time series of average temperature, relative humidity, wind speed, and direction of all sites in August 2018.

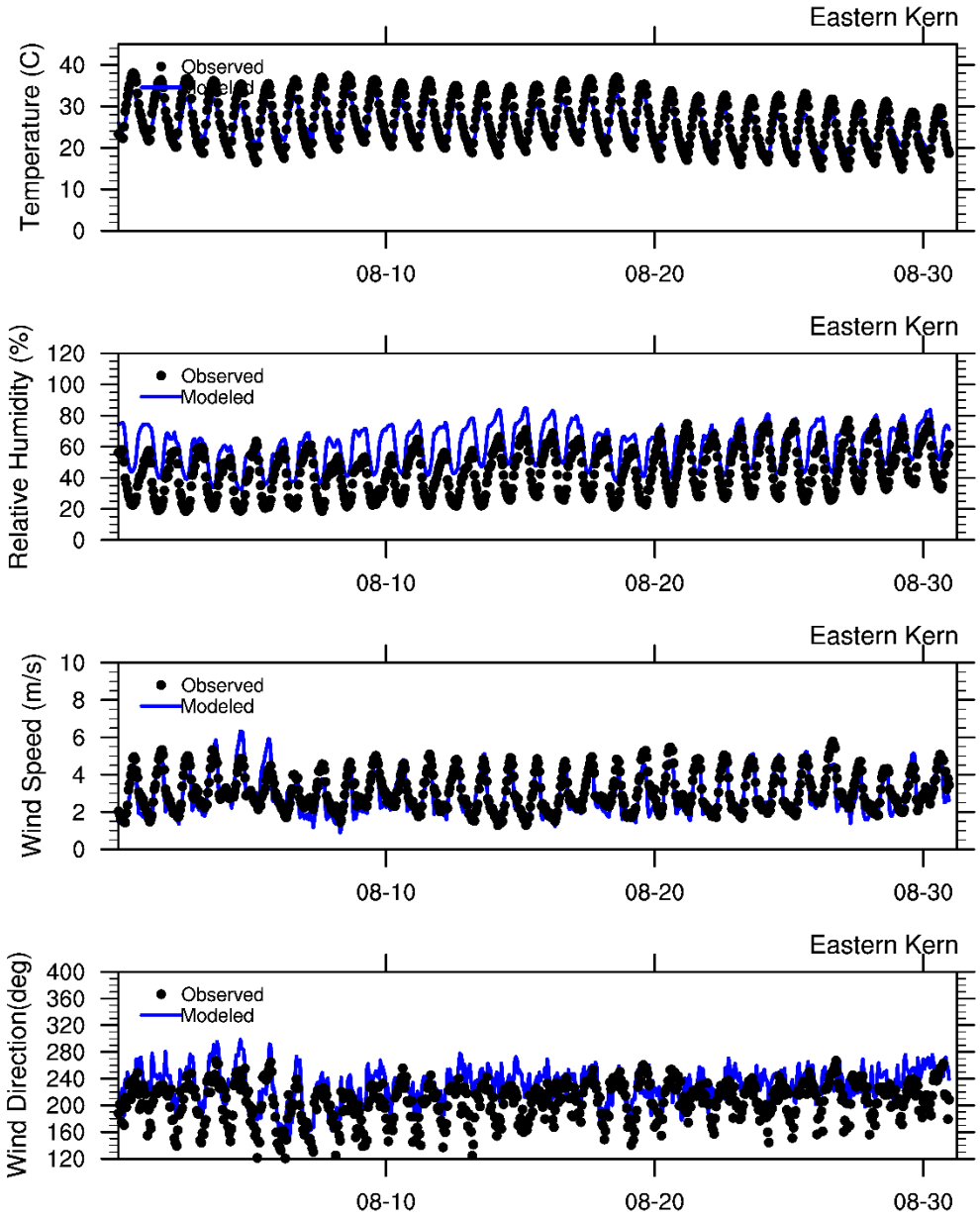

Figure S 6. Time series of average temperature, relative humidity, wind speed, and direction of all sites in September 2018.

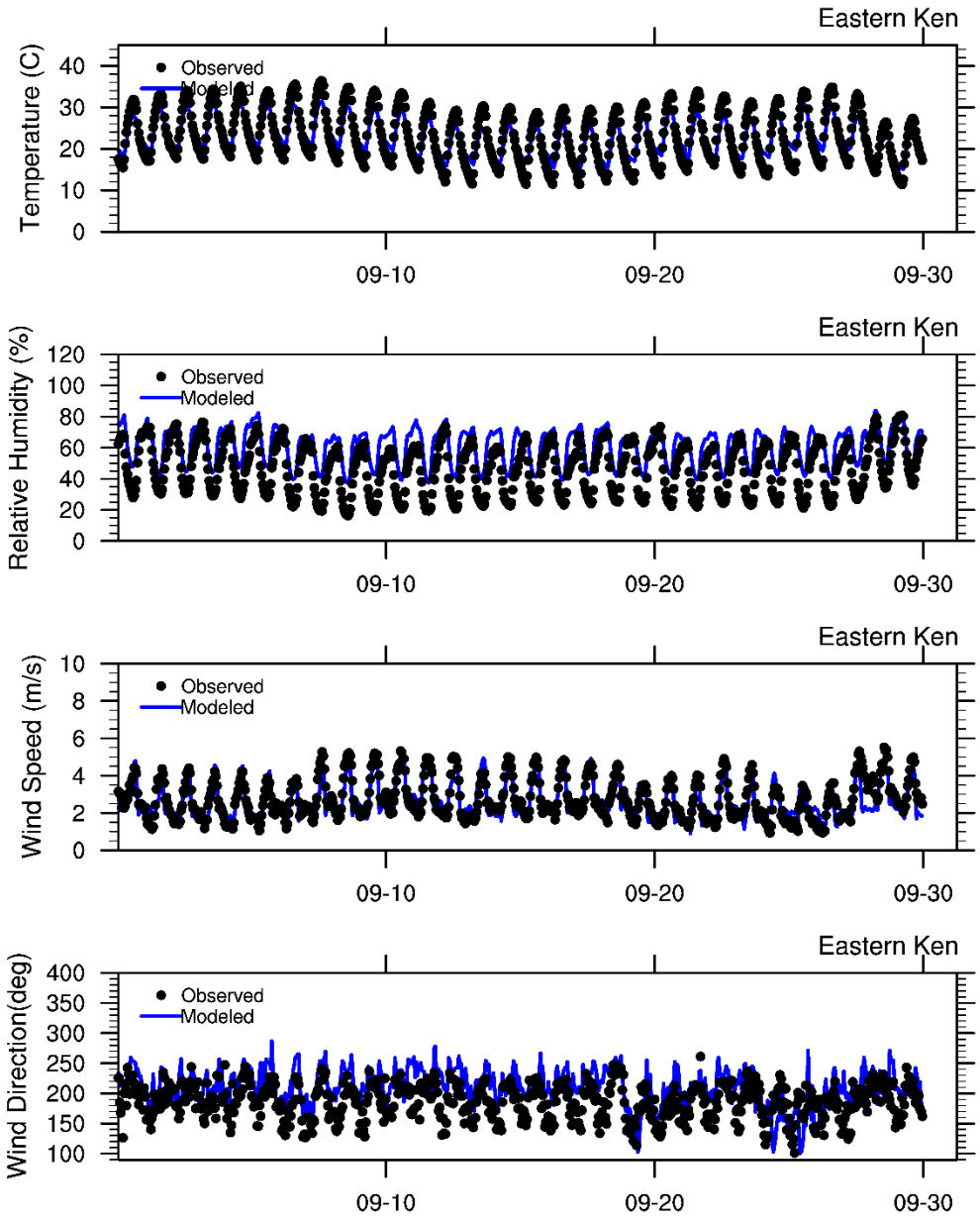

Figure S 7. Time series of average temperature, relative humidity, wind speed, and direction, and temperature of all sites in October 2018.

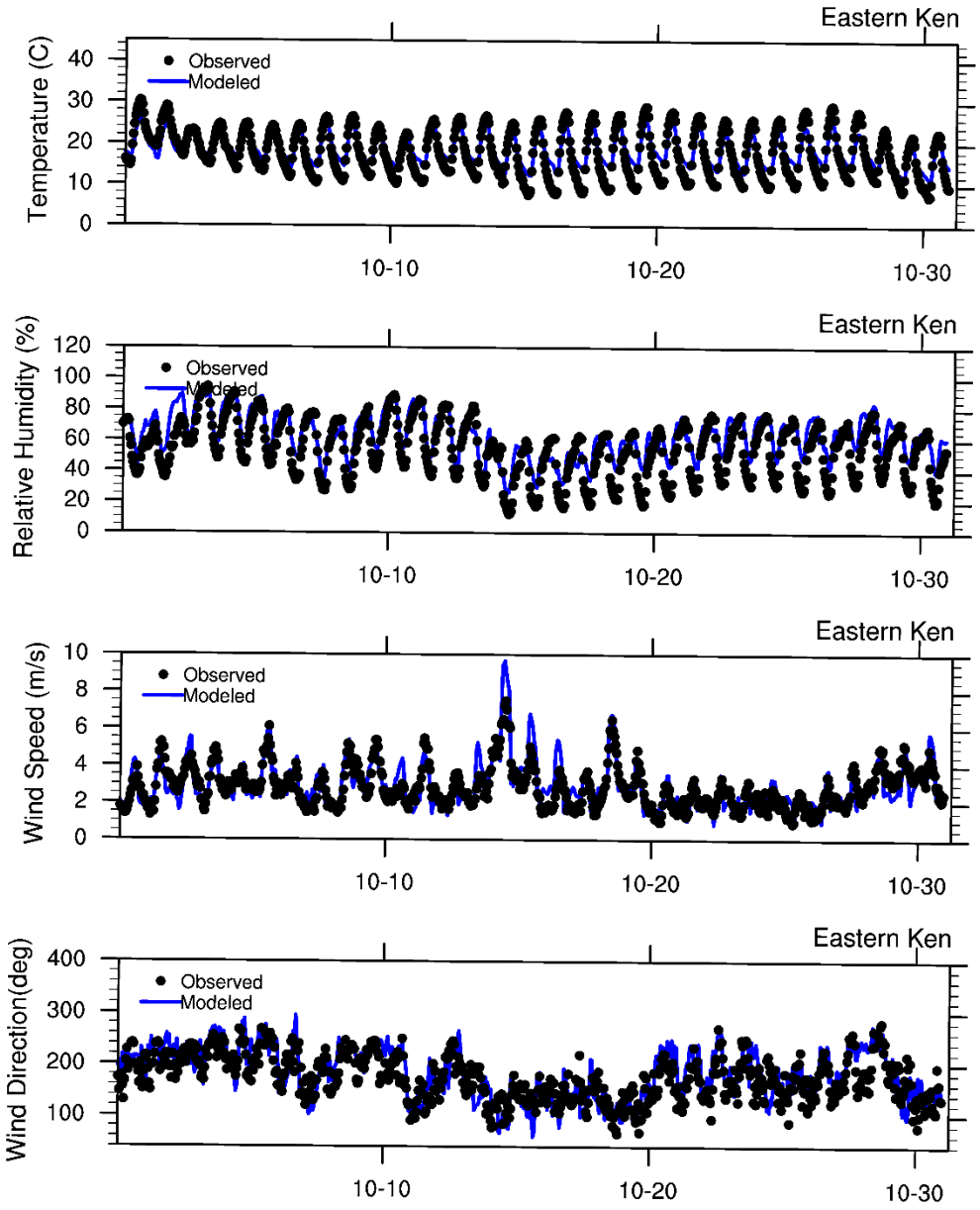

Figure S 8. Observed and modeled ozone frequency distribution at the Mojave-923PooleSt site for the ozone season (April – October 2018)

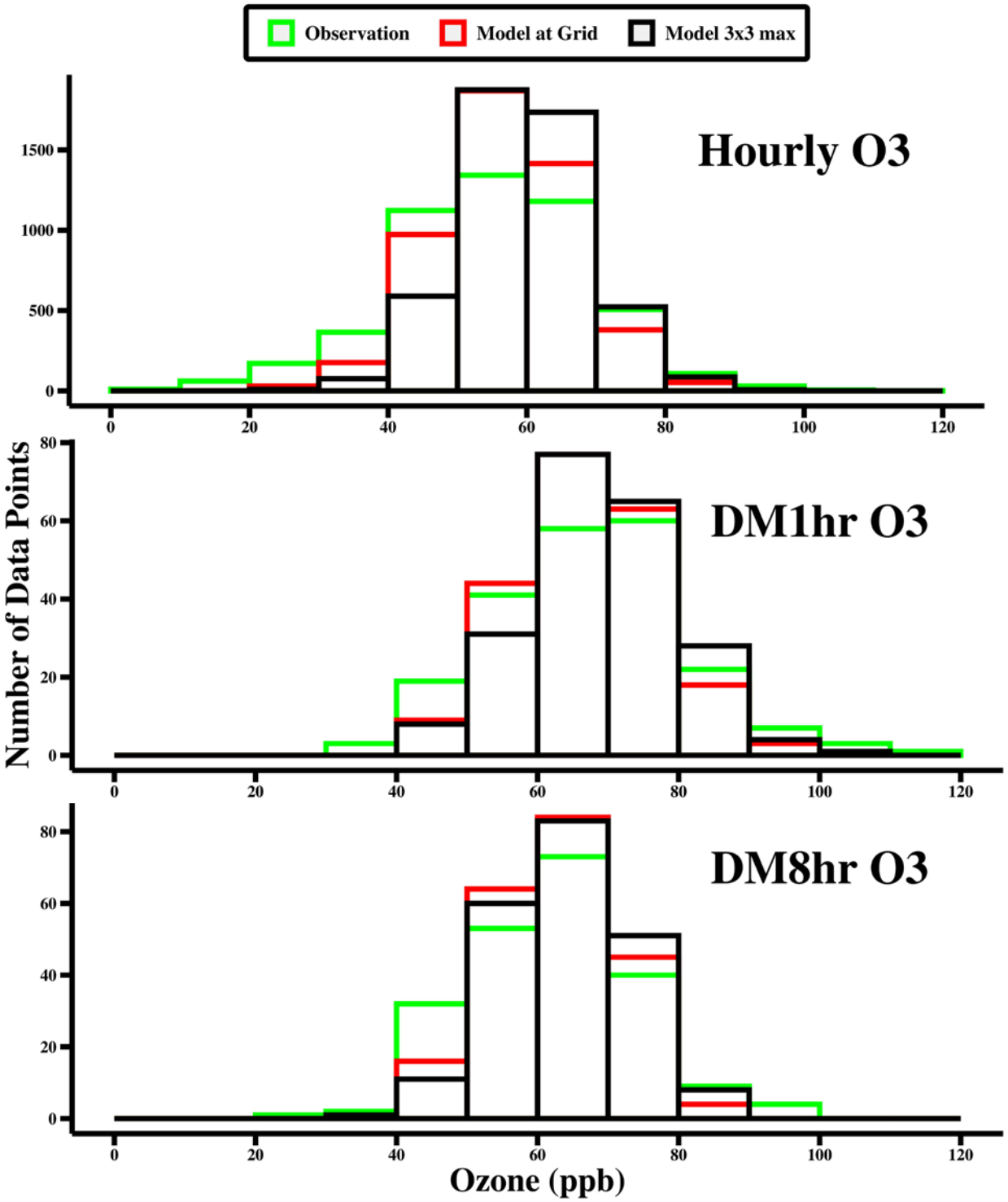

Figure S 9. Observed and modeled ozone scatter plots at the Mojave-923 PooleSt site for the ozone season (April – October 2018)

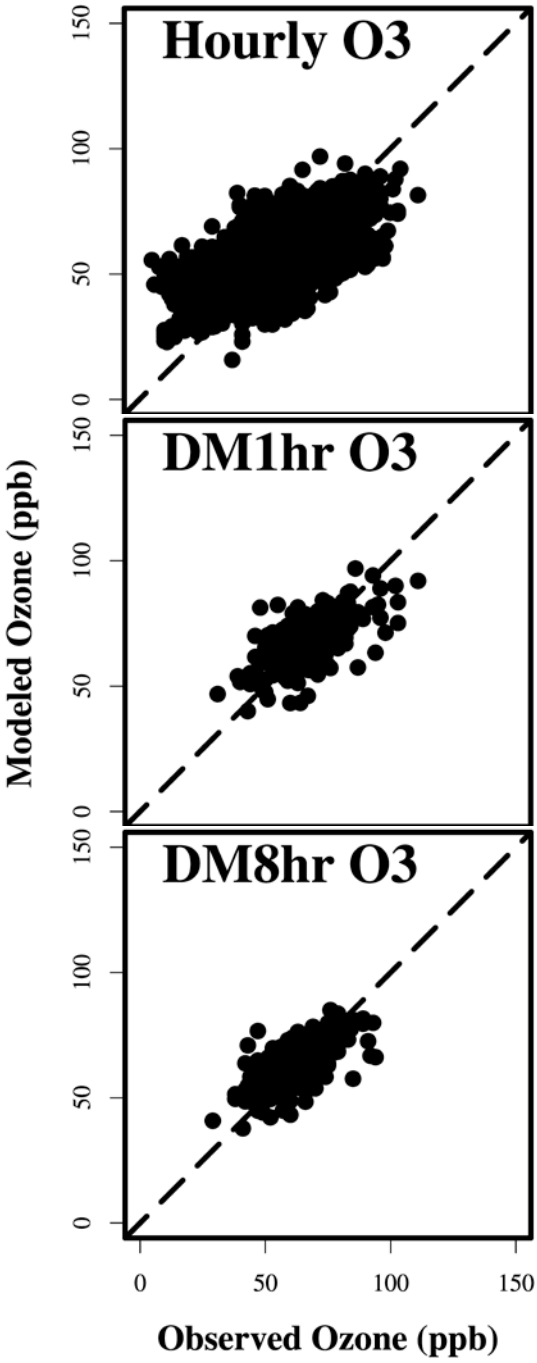

Figure S 10. Time-series of hourly ozone at Mojave-923 PooleSt for the ozone season (April – October 2018)

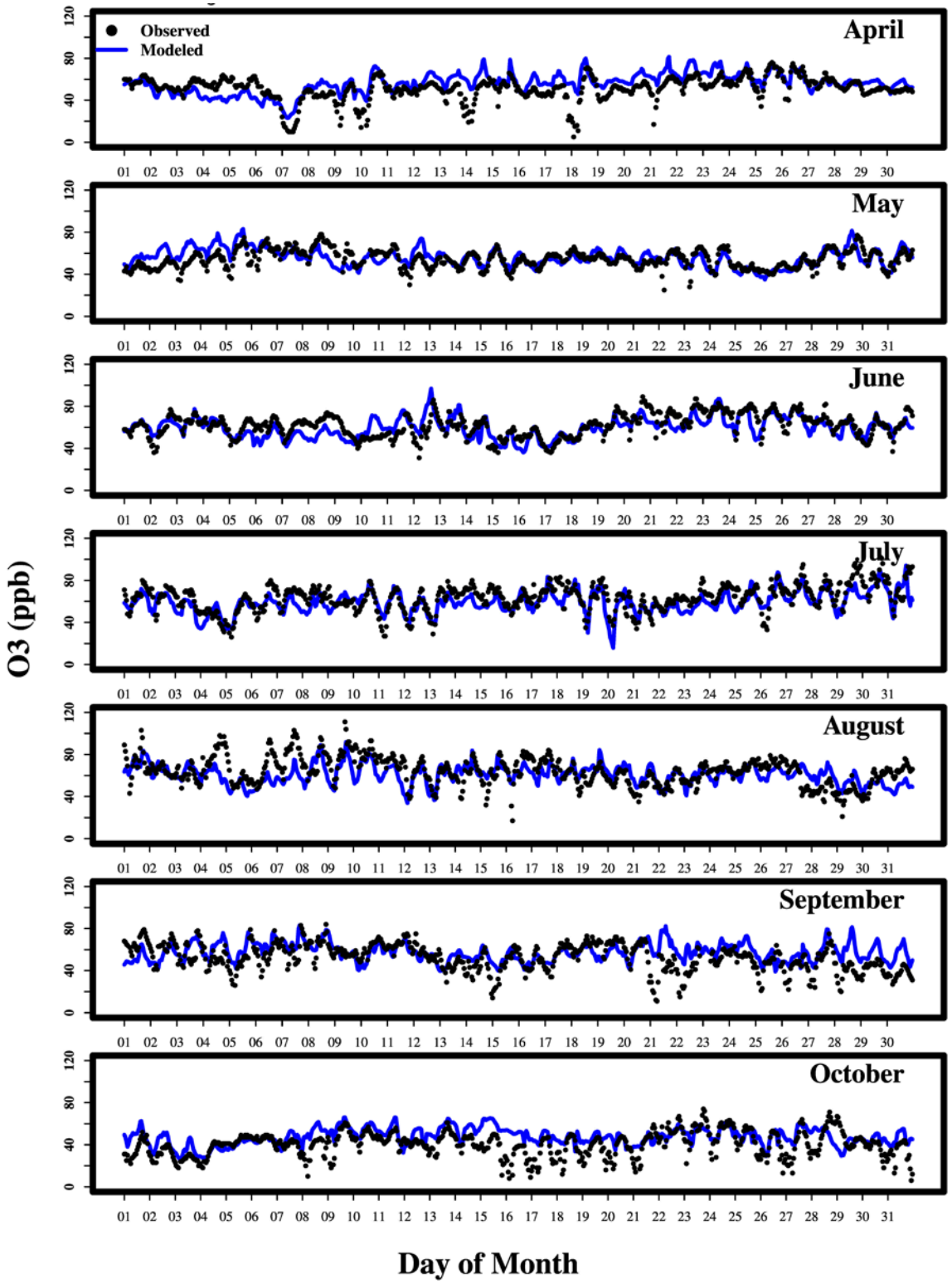

Figure S 13. Time-series of maximum daily average 1-hour ozone at the Mojave-923PooleSt site for the ozone season (April – October 2018)

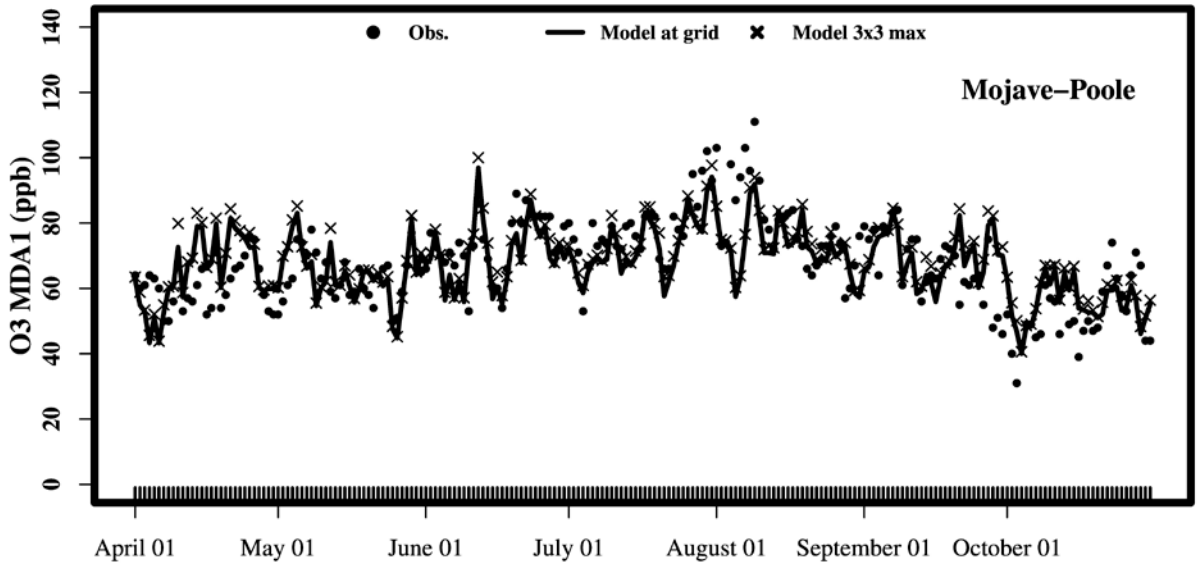

Figure S 14. Time-series of maximum daily average 8-hour ozone at the Mojave-923PooleSt site for the ozone season (April – October 2018)

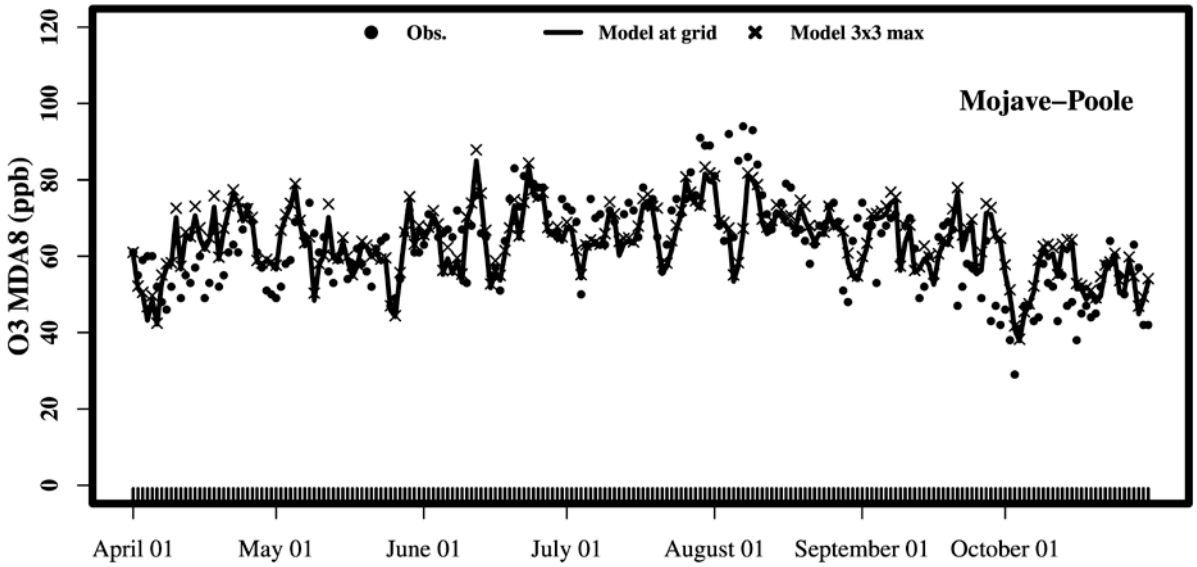

Figure S 15. Time-series of hourly NO_2 at the Shafter site in San Joaquin Valley for the ozone season (April-October 2018)

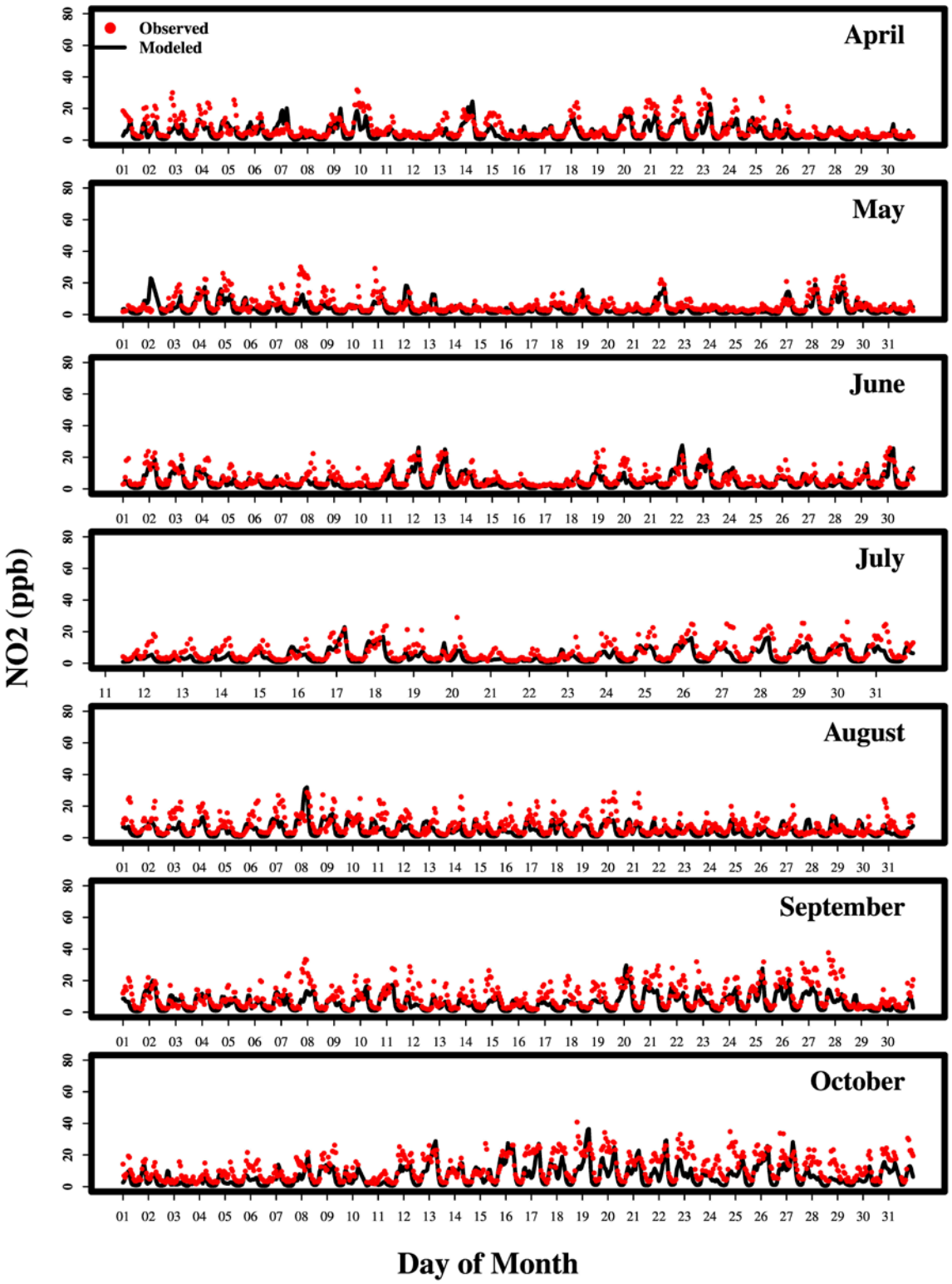

Figure S 18. Time-series of hourly NO_2 at the Santa Clarita site in South Coast for the ozone season (April-October 2018)

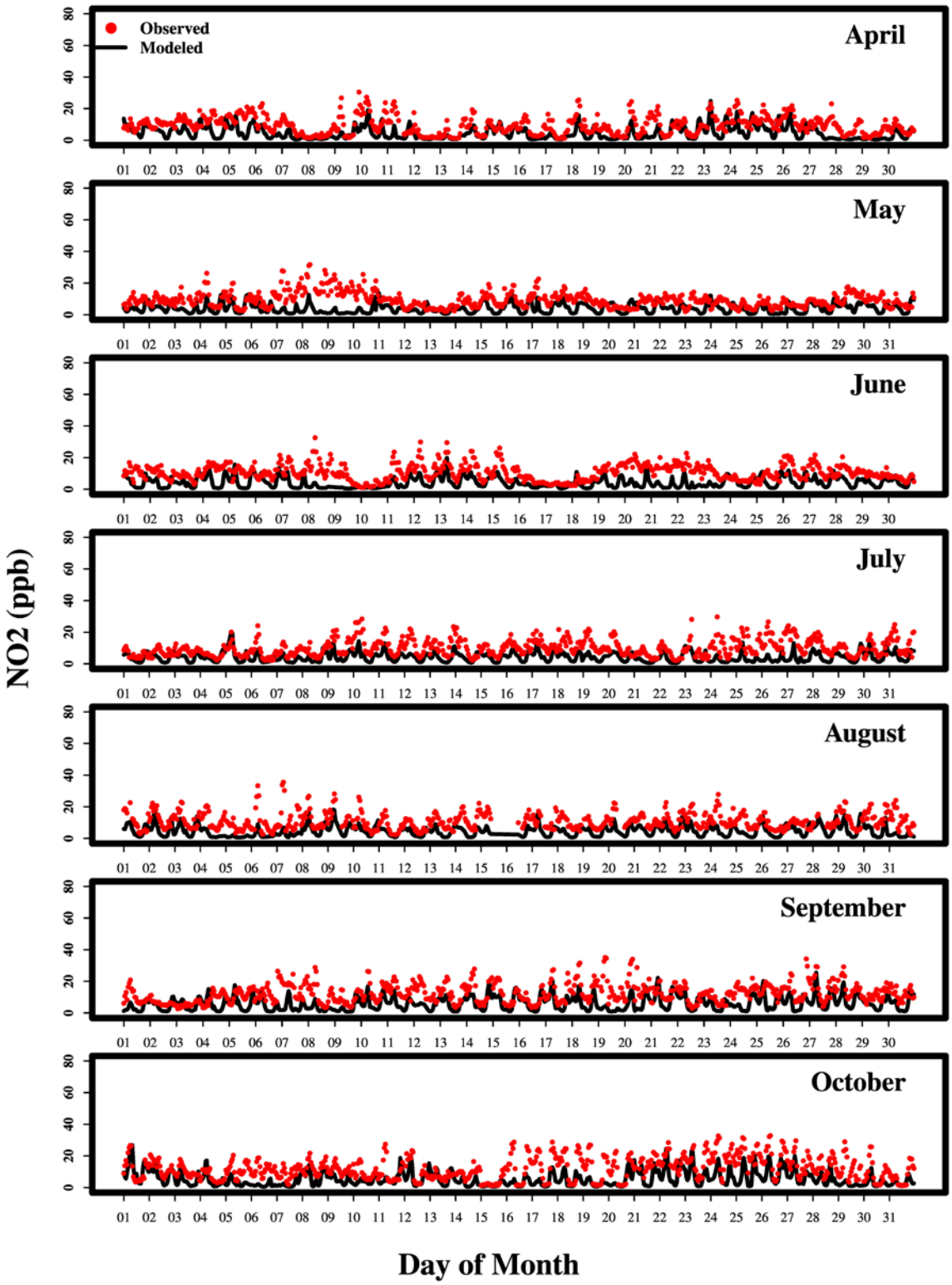

Table S 1. **List of fire days in East Kern County and SJV between year 2016 – 2019.**

East Kern 2018	SJV 2016	SJV 2017	SJV 2018	SJV 2019
2018-07-29	2016-06-30	2017-05-23	2018-07-17	2019-08-07
2018-07-30	2016-07-01	2017-05-24	2018-07-18	2019-08-15
2018-07-31	2016-07-02	2017-06-07	2018-07-24	
2018-08-04	2016-07-25	2017-06-22	2018-07-27	
2018-08-06	2016-07-26	2017-06-23	2018-07-29	
2018-08-07	2016-07-27	2017-06-25	2018-07-30	
2018-08-08	2016-07-28	2017-07-05	2018-07-31	
2018-08-09	2016-07-29	2017-07-06	2018-08-01	
2018-08-10	2016-07-30	2017-07-07	2018-08-04	
	2016-08-02	2017-07-10	2018-08-06	
	2016-08-04	2017-07-15	2018-08-07	
	2016-08-11	2017-07-23	2018-08-08	
	2016-08-12	2017-08-01	2018-08-09	
	2016-08-13	2017-08-02	2018-08-10	
	2016-08-16	2017-08-23	2018-08-16	
	2016-08-17	2017-08-25	2018-08-25	
	2016-08-18	2017-08-26		
	2016-08-19	2017-08-27		
	2016-08-20	2017-08-28		
	2016-08-29	2017-08-29		
	2016-08-30	2017-08-30		
	2016-08-31	2017-08-31		
	2016-09-07	2017-09-01		
	2016-09-08	2017-09-02		
	2016-09-18	2017-09-03		